AEDC-TR-72-134

ANALYSIS OF LAMINAR BOUNDARY LAYERS ON RIGHT CIRCULAR CONES AT ANGLE OF ATTACK, INCLUDING STREAMLINE-SWALLOWING EFFECTS

Arloe Wesley Mayne, Jr.

ARO, Inc.

October 1972

VON KÁRMÁN GAS DYNAMICS FACILITY
ARNOLD ENGINEERING DEVELOPMENT CENTER
AIR FORCE SYSTEMS COMMAND
ARNOLD AIR FORCE STATION, TENNESSEE

NOTICES

When U. S. Government drawings specifications, or other data are used for any purpose other than a definitely related Government procurement operation, the Government thereby incurs no responsibility nor any obligation whatsoever, and the fact that the Government may have formulated, furnished, or in any wav supplied the said drawings, specifications, or other data, is not to be regarded by implication or otherwise, or in any manner licensing the holder or any other person or corporation, or conveying any rights or permission to manufacture, use, or sell any patented invention that may in any way be related thereto.

Qualified users may obtain copies of this report from the Defense Documentation Center.

References to named commercial products in this report are not to be considered in any sense as an endorsement of the product by the United States Air Force or the Government.

DEPARTMENT OF THE AIR FORCE
HEADQUARTERS ARNOLD ENGINEERING DEVELOPMENT CENTER (AFSC)
ARNOLD AIR FORCE STATION, TENNESSEE 37389

TRANSMITTAL NOTE

1. The attached report is forwarded for your information and retention.

2. Inquiries relative to any feature of this report should be addressed to this Headquarters, ATTN: XON.

A. L. COAPMAN, Colonel, USAF
Director of Test

ANALYSIS OF LAMINAR BOUNDARY LAYERS ON RIGHT CIRCULAR CONES AT ANGLE OF ATTACK, INCLUDING STREAMLINE-SWALLOWING EFFECTS

Arloe Wesley Mayne, Jr.
ARO, Inc.

FOREWORD

The work reported herein was supported by Headquarters, Arnold Engineering Development Center (AEDC), Air Force Systems Command (AFSC), under Program Element 65802F.

The research presented was performed by ARO, Inc. (a subsidiary of Sverdrup & Parcel and Associates, Inc.), contract operator of AEDC, AFSC, Arnold Air Force Station, Tennessee, under Contract 40600-73-C-0004. The research was conducted from September 1970 to April 1972 under ARO Project Nos. VW5106 and VW5206, and the manuscript was submitted for publication on July 26, 1972.

This report was originally prepared as a dissertation for the University of Tennessee in partial fulfillment of the requirements for the Doctor of Philosophy degree.

This technical report has been reviewed and is approved.

ELTON R. THOMPSON
Research and Development
Division
Directorate of Technology

ROBERT O. DIETZ
Acting Director
Directorate of Technology

ABSTRACT

A method has been developed for treating the three-dimensional compressible laminar boundary-layer equations for the case of a right circular cone at angle of attack in supersonic and hypersonic flow. Swallowing by the boundary layer of the inviscid entropy layer, i.e., streamline swallowing, has been treated by means of a mass-flow balance between the inviscid and viscous flowfields. The boundary-layer equations were developed in a general Crocco-variables form and particularized to the case of a right circular cone at angle of attack. A finite-difference technique was formulated for solving the governing equations and treating the streamline-swallowing phenomenon. The resulting second-order accurate set of coupled nonlinear difference equations were solved in an iteration scheme which employed an efficient algorithm especially suited to their form. The general treatment of the problem and the method of solution were verified by the good agreement obtained between the results of the method developed and both experimental data and results from another method of computation. Results were presented which showed that, for sufficiently high Mach number and bow shock strength variations, streamline swallowing has a significant influence on computed boundary-layer data. It was concluded that streamline swallowing should be included in three-dimensional boundary-layer analyses for conical bodies under these conditions.

TABLE OF CONTENTS

LIST OF FIGURES

FIGURE PAGE

LIST OF SYMBOLS

Latin

A,B,C	Terms in general forms of finite-difference equations
AX(I), I = 1,14	Terms involving body geometry and boundary data
C_{f_ξ}, C_{f_η}	Coefficients of skin friction in ξ and η directions
c_p	Specific heat at constant pressure
G	Normalized η component of velocity
H	Total enthalpy
h_1, h_2, h_3	Metric coefficients corresponding to ξ, η, and ζ coordinates
J	Transformed ζ component of velocity
L	Reference length
M	Mach number
$\dot{m}^*$, $\dot{m}'$	Mass flow rates in inviscid and viscous flowfields
NETA	Number of mesh points in η direction
NZ	Number of mesh points in ζ direction
P,Q	Terms used in solution of finite-difference equations
p	Pressure
Pr	Prandtl number
R	Gas constant
Re	Reference Reynolds number
s	General length
St_∞	Stanton number based on freestream conditions
T	Temperature

U	Velocity in freestream
u,v,w	Velocity components in ξ, η, and ζ directions
X	Dummy variable representing ϕ, G, or θ
y	Distance normal to body surface
Z	Function of ξ and η used to introduce similarity

Greek

α	Angle of attack
α_{Xi}, $i = 1,5$	Terms appearing in general forms of governing equations
γ	Ratio of specific heats
$\Delta\zeta$	Finite-difference grid spacing in ζ direction
$\Delta\eta$	Finite-difference grid spacing in η direction
δ^*	Displacement thickness
ζ	Coordinate normal to body surface
η	Lateral coordinate
θ	Total enthalpy ratio, H/He
θ_c	Cone half-angle
λ	Dummy variable representing ξ or η
μ	Coefficient of viscosity
ξ	Longitudinal coordinate
ρ	Mass density
ϕ	Shear function

Subscripts

e	Value of outer edge of boundary layer
n	ζ-grid point location
sh	Value at shock wave

ss	Value at separating surface in inviscid flowfield
w	Value at body surface
∞	Value in freestream

Special Notation

$(\overline{\quad})$	Denotes dimensional quantity

CHAPTER I
INTRODUCTION

As indicated by the reviews of the literature by Cooke and Hall (1)[1] and Stewartson (2), there exists a large body of work dealing with three-dimensional boundary-layer flows. In spite of this large body of literature, a number of significant areas in three-dimensional boundary-layer theory remain relatively unexplored. Although this statement is especially true for turbulent boundary layers, the present work is directed toward laminar boundary layers, as only a heuristic treatment of three-dimensional turbulent boundary layers currently appears feasible.

In comparison with the two-dimensional and axisymmetric flow situations, relatively little rigorous work has been done on the computation of the three-dimensional boundary-layer flow over even simple axisymmetric bodies at angle of attack, and most of that has involved treatment of only the most windward line of a body, e.g., Libby (3). Because of the simplifications introduced by the spanwise derivatives' being zero, the case of the three-dimensional boundary layer on a yawed infinite cylinder has received considerable attention, as in the report by Reshotko and Beckwith (4). Another case which has received considerable attention because of its simplifying features is that of the

---

[1]Numbers in parentheses refer to similarly numbered references in the bibliography.

three-dimensional boundary layer on a conical body. In this case the classical treatment of the problem is such that the governing equations may be transformed to eliminate the dependence on the streamwise independent variable, as has been done by McGowan and Davis (5).

In addition to the special cases just mentioned, some computations have been performed for more general three-dimensional boundary layers; however, in many instances these computations have been based on the small crossflow assumptions. The small crossflow assumptions involve assuming that the boundary-layer velocity component normal to the inviscid body-surface streamlines and all derivatives of this velocity component are everywhere zero. These assumptions permit considerable simplification of the governing equations; however, the results of Moore and DeJarnette (6) have shown that, for cases of interest to them, the use of the small crossflow assumptions leads to errors of approximately ten percent in computed surface heat-transfer and skin-friction data, when compared to more exact calculations.

It can be seen that most treatments of three-dimensional boundary layers deal with special cases which permit simplification of the problem because of either the restrictions of the physical problem or assumptions made in the governing equations, and that there are many significant areas remaining to be investigated. Consideration of phenomena such as variable wall temperature, surface mass transfer, and chemically reacting flows have not yet been generally delved into, even if in principle the approach is understood.

The problem of streamline swallowing by the boundary layer on

blunt bodies in supersonic or hypersonic flow is one which has received considerable attention in the cases of both two-dimensional and axially symmetric flow, e.g., Ferri (7) and Mayne and Adams (8). This same effect exists for blunt-nosed axisymmetric bodies at angle of attack, as noted by Fannelop and Waldman (9); however, this complicated problem has not yet been treated. In addition to these blunt-body cases, there is also an effect of streamline swallowing in the boundary-layer flow around a sharp conical body at angle of attack in supersonic and hypersonic flow, and, although it has not yet been investigated, this problem is amenable to analytical treatment.

For the case of flow over a two-dimensional or unyawed axisymmetric blunt body, the streamline-swallowing phenomenon may be demonstrated by first considering that in the classical treatment of the boundary-layer problem, the outer-edge boundary conditions for the boundary-layer equations are taken to be the conditions at the body surface calculated by inviscid techniques. This is equivalent to assuming that all of the flow along the outer edge of the boundary layer crossed the normal portion of the bow shock wave. In reality, however, as the flow proceeds along the body, and the boundary layer entrains fluid, the portion of the flow which crossed the blunter forward part of the shock wave will be "swallowed" by the boundary layer, as indicated in Figure 1. The flow along the outer edge of the boundary layer on the aft portion of the body will have passed through an oblique part of the shock wave, and will be at a different state than had it passed through a normal shock wave. Naturally, the use of the outer-edge boundary conditions resulting

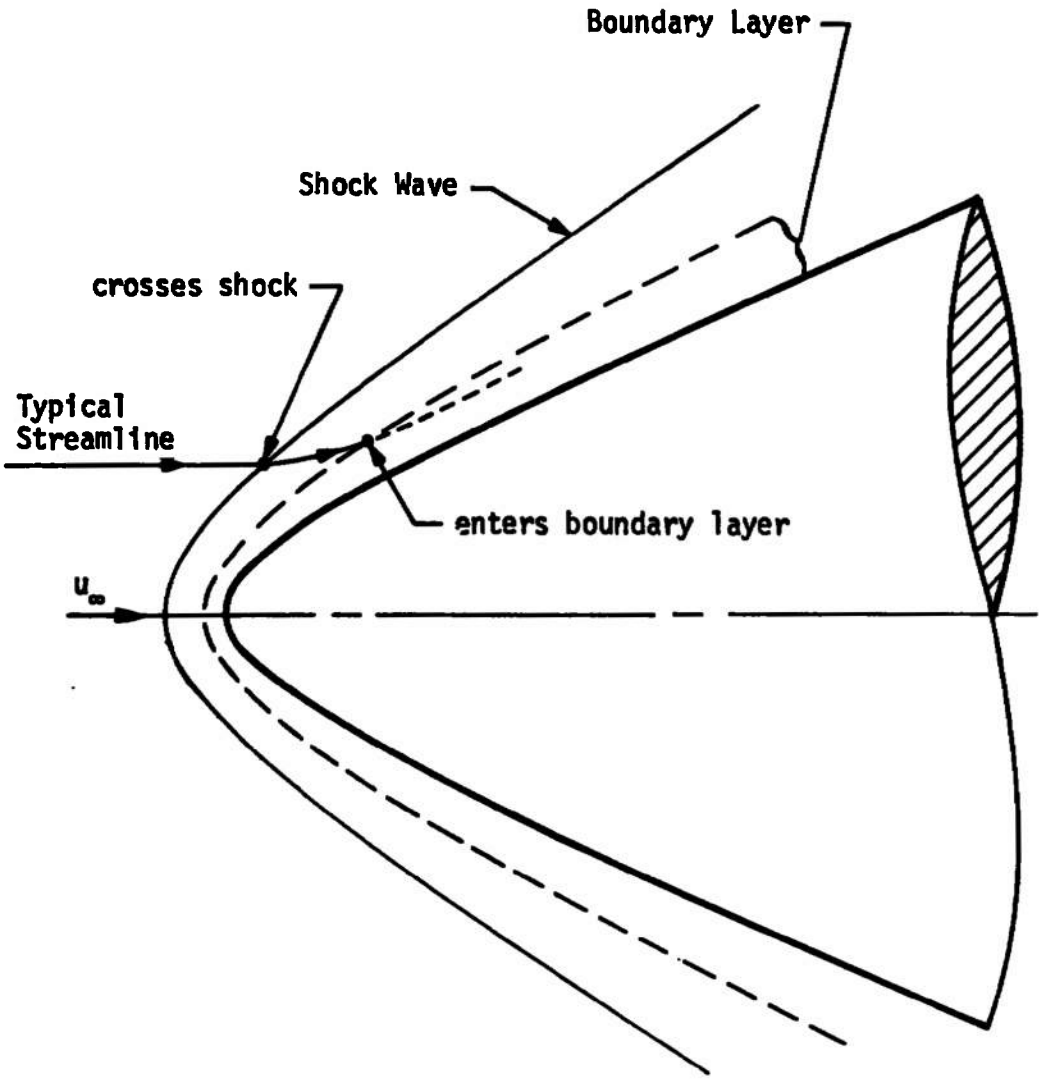

Figure 1. Streamline Swallowing on Blunt Axisymmetric Body at Zero Angle of Attack

from considering the streamline swallowing yields solutions to the boundary-layer equations which differ from those solutions obtained using the classical treatment of the outer-edge boundary conditions. References 7 and 8 show significant effects of the streamline swallowing on computed boundary-layer profile data, surface heat transfer rate, and skin friction.

For the case of supersonic or hypersonic flow over a right circular cone at angle of attack, the streamline-swallowing phenomenon is caused by the entrainment by the boundary layer of the lateral flow around the cone. (Certainly this discussion applies to a more general class of sharp bodies; however, a simple description of that class of bodies is not possible.) The conventional treatment of this boundary-layer problem involves using the inviscid body-surface conditions for the outer-edge boundary conditions. This is equivalent to assuming that the flow along the outer edge of the boundary layer all crossed the most windward (and bluntest) part of the shock wave. In fact, however, the flow which crossed the blunter portion of the shock wave is swallowed by the boundary layer, as shown in Figure 2. A more proper treatment of the outer-edge boundary conditions, as noted by DaForno (10), would be to take into account the swallowing of the inviscid flow by the boundary layer. This can be done by an appropriate mass balance between the boundary layer and the inviscid flowfield, such that the resulting boundary conditions applied along the outer edge of the boundary layer properly reflect the entrainment process.

The purpose of this work is an analytical investigation into

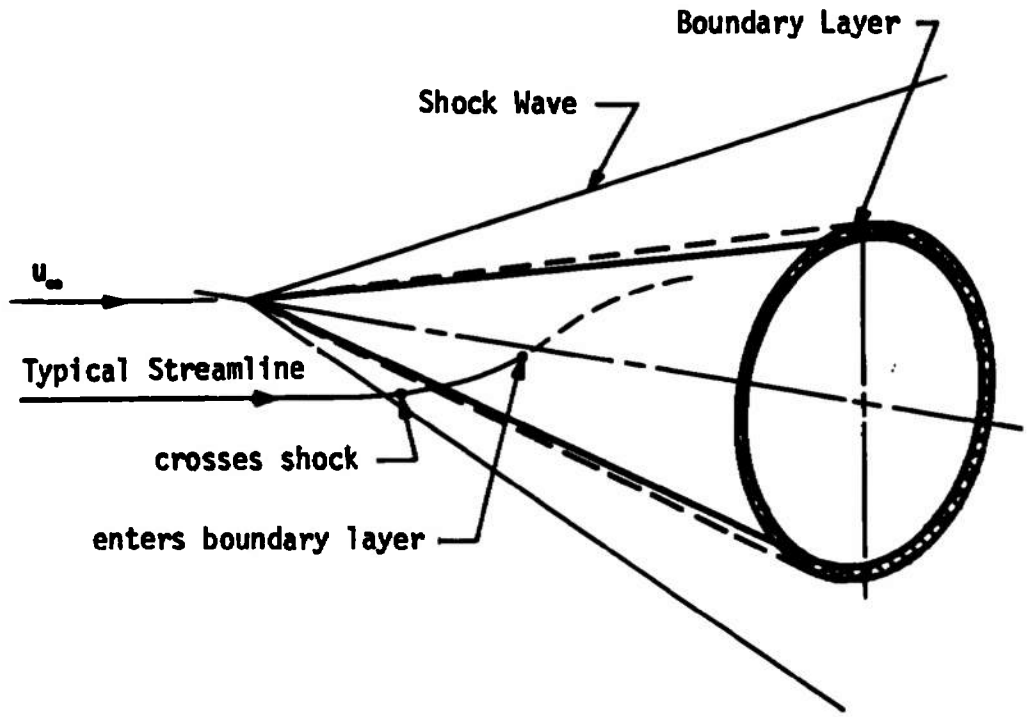

Figure 2. Streamline Swallowing on Right Circular Cone at Angle of Attack

the effects of streamline swallowing on solutions to the three-dimensional boundary-layer equations for cases of supersonic and hypersonic flow over right circular cones at angle of attack. The following chapters will present the transformation of the governing equations into a tractable form, a method for their solution, and the results of calculations which have been performed.

CHAPTER II
FORMULATION OF THE PROBLEM

In this chapter are presented the governing equations for three-dimensional compressible laminar boundary-layer flow, the transformation of these equations into a tractable form, and a discussion of the boundary conditions required to solve the equations, especially as determined through the streamline-swallowing treatment. The boundary-layer equations are first presented in a general metric form; these equations are then nondimensionalized and transformed into a Crocco-variables form. Since the three-dimensional boundary-layer equations in the present Crocco-variables form have not been presented elsewhere, the equations developed in this chapter are not based on any particular body geometry, so that they may be applied to any desired body.

The gas under consideration is assumed to be both thermally and calorically perfect. The governing partial differential equations which are presented are the continuity equation, a longitudinal momentum equation, a lateral momentum equation, and an energy equation. The perfect gas equation of state and a viscosity law complete the set of governing equations. The Crocco transformation is used to eliminate the component of velocity normal to the body surface as a dependent variable, and, thereby, to reduce the number of partial differential equations which must be solved from four to three. The spirit of the treatment

given herein to the boundary-layer equations follows the work of Raetz (11), who made the first significant advance into the solution of general three-dimensional compressible laminar boundary-layer problems.

Streamline swallowing by the boundary layer is treated by determining the outer-edge boundary conditions for the boundary-layer equations through a mass balance between the boundary layer and the inviscid flowfield over the body. The outer-edge boundary conditions required for solving the boundary-layer equations are obtained through the streamline-swallowing treatment from the results of inviscid flowfield computations made using the method of Jones (12) for supersonic and hypersonic flow over conical bodies at angle of attack. Boundary-layer displacement effects (i.e., boundary-layer influences on the inviscid flowfield) are neglected in the treatment of the problem considered herein.

I. METRIC FORM OF THE BOUNDARY-LAYER EQUATIONS AND A PRELIMINARY TRANSFORMATION

The three-dimensional compressible laminar boundary-layer equations can be obtained from the Navier-Stokes equations by an order-of-magnitude analysis in which only the dominant terms in the equations are retained. This analysis can be conveniently accomplished in the general orthogonal (ξ,η,ζ) coordinate system indicated in Figure 3, where ξ and η are defined in the surface over which the boundary layer flows, and ζ is a coordinate normal to the surface. On this surface ζ is a constant, usually zero. For this coordinate system the general element of length is

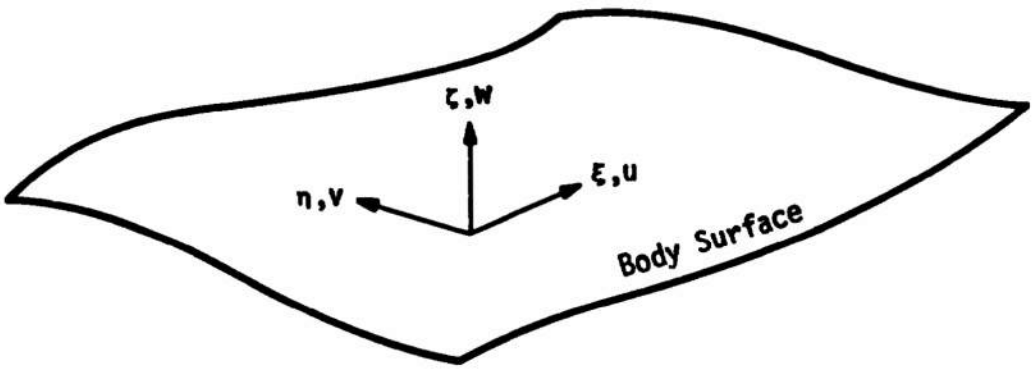

Figure 3. Orthogonal Coordinate System and Velocity Components for Boundary-Layer Equations

$$(d\bar{s})^2 = \bar{h}_1^2\,(d\xi)^2 + \bar{h}_2^2\,(d\eta)^2 + \bar{h}_3^2\,(d\zeta)^2 \tag{1}$$

where the bar over a quantity designates a dimensional quantity. It is assumed herein that $\bar{h}_1$ and $\bar{h}_2$ are functions of only ξ and η; this assumption should be valid so long as the surface is not excessively curved in comparison to the boundary-layer thickness. The metric coefficient $\bar{h}_3$ is generally a function of ξ, η, and ζ; $\bar{h}_3 d\zeta$ is a differential element of the physical distance normal to the body surface, i.e., $\bar{h}_3 d\zeta = d\bar{y}$.

For a perfect gas, at steady state, with no body forces, in this non-rotating coordinate system, the three-dimensional compressible laminar boundary-layer equations, as given by Mager (13), for example, are:

Continuity

$$\frac{\partial}{\partial\xi}(\bar{h}_2\bar{h}_3\,\bar{\rho}\,\bar{u}) + \frac{\partial}{\partial\eta}(\bar{h}_1\bar{h}_3\,\bar{\rho}\,\bar{v}) + \frac{\partial}{\partial\zeta}(\bar{h}_1\bar{h}_2\,\bar{\rho}\,\bar{w}) = 0 \tag{2}$$

ξ Momentum

$$\frac{\bar{u}}{\bar{h}_1}\frac{\partial\bar{u}}{\partial\xi} + \frac{\bar{v}}{\bar{h}_2}\frac{\partial\bar{u}}{\partial\eta} + \frac{\bar{w}}{\bar{h}_3}\frac{\partial\bar{u}}{\partial\zeta} + \frac{\bar{u}}{\bar{h}_1}\frac{\bar{v}}{\bar{h}_2}\frac{\partial\bar{h}_1}{\partial\eta} - \frac{\bar{v}^2}{\bar{h}_1\bar{h}_2}\frac{\partial\bar{h}_2}{\partial\xi} = -\frac{1}{\bar{\rho}\bar{h}_1}\frac{\partial\bar{p}}{\partial\xi} + \frac{1}{\bar{\rho}\bar{h}_3}\frac{\partial}{\partial\zeta}\left(\frac{\bar{\mu}}{\bar{h}_3}\frac{\partial\bar{u}}{\partial\zeta}\right) \tag{3}$$

η Momentum

$$\frac{\bar{u}}{\bar{h}_1}\frac{\partial\bar{v}}{\partial\xi} + \frac{\bar{v}}{\bar{h}_2}\frac{\partial\bar{v}}{\partial\eta} + \frac{\bar{w}}{\bar{h}_3}\frac{\partial\bar{v}}{\partial\zeta} + \frac{\bar{u}\,\bar{v}}{\bar{h}_1\bar{h}_2}\frac{\partial\bar{h}_2}{\partial\xi} - \frac{\bar{u}^2}{\bar{h}_1\bar{h}_2}\frac{\partial\bar{h}_1}{\partial\eta} = -\frac{1}{\bar{\rho}\bar{h}_2}\frac{\partial\bar{p}}{\partial\eta} + \frac{1}{\bar{\rho}\bar{h}_3}\frac{\partial}{\partial\zeta}\left(\frac{\bar{\mu}}{\bar{h}_3}\frac{\partial\bar{v}}{\partial\zeta}\right) \tag{4}$$

Energy

$$\frac{\bar{u}}{\bar{h}_1}\frac{\partial \bar{H}}{\partial \xi} + \frac{\bar{v}}{\bar{h}_2}\frac{\partial \bar{H}}{\partial \eta} + \frac{\bar{w}}{\bar{h}_3}\frac{\partial \bar{H}}{\partial \zeta}$$

$$= \frac{1}{\bar{\rho}\,\bar{h}_3}\frac{\partial}{\partial \zeta}\left[\frac{\bar{\mu}}{Pr\,\bar{h}_3}\frac{\partial \bar{H}}{\partial \zeta} - \frac{1}{2}\frac{\bar{\mu}}{\bar{h}_3}\frac{(1-Pr)}{Pr}\frac{\partial}{\partial \zeta}(\bar{u}^2 + \bar{v}^2)\right] \tag{5}$$

The boundary-layer form of the ζ-momentum equation is $\frac{\partial \bar{p}}{\partial \zeta} = 0$. This yields a constant pressure across the boundary layer, having the value of the pressure imposed along the outer edge of the boundary layer.

The equation of state and the viscosity law may be written as

Equation of State

$$\bar{p} = \bar{\rho}\,\bar{R}\,\bar{T} \tag{6}$$

Viscosity Law

$$\bar{\mu} = \bar{\mu}\,(\bar{T}) \tag{7}$$

The following equation relates the total enthalpy to the temperature and the kinetic energy of the flow. In keeping with the boundary-layer assumptions, the kinetic energy of the motion in the directional normal to the wall is neglected.

$$\bar{H} = \bar{c}_p\,\bar{T} + \frac{1}{2}(\bar{u}^2 + \bar{v}^2) \tag{8}$$

Equations (2) through (8) are the equations governing three-dimensional compressible laminar boundary-layer flow, under the assumptions which have been given. The dependent variables are $\bar{u}$, $\bar{v}$, $\bar{w}$, $\bar{H}$, $\bar{\rho}$, $\bar{\mu}$, and $\bar{T}$.

Equations (2) through (8) are now cast into a nondimensional form according to the following scheme:

$$h_1 = \frac{\bar{h}_1}{\bar{L}} \qquad \mu = \frac{\bar{\mu}}{\bar{\mu}_\infty}$$

$$h_2 = \frac{\bar{h}_2}{\bar{L}} \qquad p = \frac{\bar{p}}{\bar{\rho}_\infty \bar{u}_\infty^2}$$

$$h_3 = \frac{\bar{h}_3 \sqrt{Re}}{\bar{L}} \qquad \rho = \frac{\bar{\rho}}{\bar{\rho}_\infty}$$

$$u = \frac{\bar{u}}{\bar{u}_\infty} \qquad T = \frac{\bar{T}\,\bar{c}_p}{\bar{u}_\infty^2}$$

$$v = \frac{\bar{v}}{\bar{u}_\infty} \qquad H = \frac{\bar{H}}{\bar{u}_\infty^2}$$

$$w = \frac{\bar{w}\ \sqrt{Re}}{\bar{u}_\infty} \tag{9}$$

where

$$Re = \frac{\bar{\rho}_\infty \bar{u}_\infty \bar{L}}{\bar{\mu}_\infty}$$

The Reynolds number factor appearing in the relations for h_3 and w is not necessary to nondimensionalize these variables; however, it does serve to eliminate any explicit dependence of the resulting equations on the freestream Reynolds number.

The application of Equations (9) to Equations (2) through (8) yields the following set of nondimensional equations:

Continuity

$$\frac{\partial}{\partial \xi}\ (h_2 h_3\ \rho\ u) + \frac{\partial}{\partial \eta}\ (h_1 h_3\ \rho\ v) + \frac{\partial}{\partial \zeta}\ (h_1 h_2\ \rho\ w) = 0 \tag{10}$$

ξ Momentum

$$\frac{u}{h_1}\ \frac{\partial u}{\partial \xi} + \frac{v}{h_2}\ \frac{\partial u}{\partial \eta} + \frac{w}{h_3}\ \frac{\partial u}{\partial \zeta} + \frac{uv}{h_1 h_2}\ \frac{\partial h_1}{\partial \eta}$$

$$- \frac{v^2}{h_1 h_2}\ \frac{\partial h_2}{\partial \xi} = - \frac{1}{\rho h_1}\ \frac{\partial p}{\partial \xi} + \frac{1}{\rho h_3}\ \frac{\partial}{\partial \zeta}\left(\frac{\mu}{h_3}\ \frac{\partial u}{\partial \zeta}\right) \tag{11}$$

η Momentum

$$\frac{u}{h_1}\ \frac{\partial v}{\partial \xi} + \frac{v}{h_2}\ \frac{\partial v}{\partial \eta} + \frac{w}{h_3}\ \frac{\partial v}{\partial \zeta} + \frac{uv}{h_1 h_2}\ \frac{\partial h_2}{\partial \xi}$$

$$- \frac{u^2}{h_1 h_2}\ \frac{\partial h_1}{\partial \eta} = - \frac{1}{\rho h_2}\ \frac{\partial p}{\partial \eta} + \frac{1}{\rho h_3}\ \frac{\partial}{\partial \zeta}\left(\frac{\mu}{h_3}\ \frac{\partial v}{\partial \zeta}\right) \tag{12}$$

Energy

$$\frac{u}{h_1}\ \frac{\partial H}{\partial \xi} + \frac{v}{h_2}\ \frac{\partial H}{\partial \eta} + \frac{w}{h_3}\ \frac{\partial H}{\partial \zeta}$$

$$= \frac{1}{\rho h_3}\ \frac{\partial}{\partial \zeta}\left[\frac{\mu}{Pr\ h_3}\ \frac{\partial H}{\partial \zeta} - \frac{1}{2}\ \frac{\mu}{h_3}\ \frac{(1-Pr)}{Pr}\ \frac{\partial}{\partial \zeta}\ (u^2 + v^2)\right] \tag{13}$$

Equation of State

$$p = \frac{\gamma-1}{\gamma} \rho T \tag{14}$$

Viscosity Law

$$\mu = \mu(T) \tag{15}$$

Equation (8) has the nondimensional form

$$H = T + \frac{1}{2}(u^2 + v^2) \tag{16}$$

In obtaining Equation (14), the relationship $\overline{R} = \frac{\gamma-1}{\gamma} \overline{c_p}$ has been employed.

II. THE CROCCO TRANSFORMATION

In this section Equations (10) through (13) are transformed according to a transformation introduced by Crocco (14). This transformation is accomplished by letting the coordinate normal to the body surface be defined to be the longitudinal velocity component, or, in the present treatment, a normalized form of the longitudinal velocity. This yields the convenient limits of zero and unity for the normal coordinate. (The term "longitudinal" is used to refer to the ξ direction, and "lateral" is used to refer to the η direction. The term "normal" refers, of course, to the ζ direction.) The velocity component normal to the body surface is eliminated from the equations by combining the longitudinal momentum equation with each of the continuity, lateral momentum, and energy equations. This results in eliminating one of the partial

differential equations entirely. As a part of the transformation, a form of the longitudinal component of the shearing stress becomes the dependent variable associated with the transformed longitudinal momentum equation.

The Crocco transformation is accomplished by first introducing the following definitions:

$$\zeta = \frac{u}{u_e}$$

$$G = \frac{v}{v_e}$$

$$J = \frac{wZ}{u_e}$$

$$\theta = \frac{H}{H_e}$$

$$\phi = \frac{\mu Z}{h_3} \tag{17}$$

where Z is a function of ξ and η which can be defined for a particular case so as to eliminate singularities at a stagnation point or sharp tip of a body, or to introduce similarity into certain cases. The subscript "e" refers to the value of a variable at the outer edge of the boundary layer; quantities so designated are functions of only ξ and η. In order for the Crocco transformation to be meaningful, it is necessary that u increase monotonically from zero at the body surface to u_e at the outer edge of the boundary layer.

The independent variables in the transformed equations are ξ, η, and $\zeta = \frac{u}{u_e}$. The dependent variables associated with the transformed

differential equations are G, J, θ, and Φ, although J is eliminated from the equations. Through the definitions of the coordinate ζ and the metric coefficient h_3, Φ is proportional to the longitudinal component of the shearing stress.

The nondimensional temperature may be obtained from Equations (16) and (17) as

$$T = H_e\,\theta - \frac{1}{2}\left(\zeta^2\,u_e^2 + G^2\,v_e^2\right) \tag{18}$$

For convenience the temperature is retained in the transformed differential equations, although it is an explicit function of the edge conditions and the primary dependent variables. The nondimensional viscosity is treated similarly.

Application of the transformations given in Equation (17) to the ξ-momentum equation yields the following equation for the transformed velocity component normal to the body surface:

$$J = \frac{\gamma-1}{\gamma}\,\frac{1}{u_e}\,\frac{T}{p}\,\frac{\partial\Phi}{\partial\zeta} - \frac{\gamma-1}{\gamma}\,\frac{\mu Z^2}{u_e^2\,\Phi}\,\frac{T}{ph_1}\,\frac{\partial p}{\partial\xi} - \frac{\mu Z^2\,\zeta^2}{u_e\Phi\,h_1}\,\frac{\partial u_e}{\partial\xi} - \frac{\mu Z^2\,v_e\,\zeta\,G}{u_e\,\Phi\,h_2}\,\frac{\partial \ell n\,(u_e h_1)}{\partial\eta} + \frac{\mu Z^2\,v_e^2\,G^2}{u_e^2\,\Phi\,h_1 h_2}\,\frac{\partial h_2}{\partial\xi} \tag{19}$$

Application of the transformations given by Equations (17) to Equation (10), together with the introduction of Equation (19), yields the following equation which may be considered to be the transformed ξ-momentum equation:

$$\frac{\partial^2\Phi}{\partial\zeta^2} + \alpha_{\phi 1}\frac{\partial\Phi}{\partial\zeta} + \alpha_{\phi 2}\ \Phi + \alpha_{\phi 3} + \alpha_{\phi 4}\frac{\partial\Phi}{\partial\xi} + \alpha_{\phi 5}\frac{\partial\Phi}{\partial\eta} = 0 \tag{20}$$

where

$$\alpha_{\phi 1} = AX(5)\frac{\mu\zeta^2}{\Phi^2 T} + AX(6)\frac{\mu\zeta G}{\Phi^2 T} - AX(7)\frac{\mu G^2}{\Phi^2 T} + AX(8)\frac{\mu}{\Phi^2}$$

$$\alpha_{\phi 2} = 0$$

$$\alpha_{\phi 3} = \frac{\mu}{\Phi T}\Bigg\{AX(1)\frac{\zeta}{\mu}\frac{\partial\mu}{\partial\xi} - AX(1)\frac{\zeta}{T}\frac{\partial T}{\partial\xi}$$

$$+ AX(2)\frac{\partial G}{\partial\eta} + AX(2)\frac{G}{\mu}\frac{\partial\mu}{\partial\eta} - AX(2)\frac{G}{T}\frac{\partial T}{\partial\eta}$$

$$+ AX(3)\zeta + AX(4)G - AX(5)2\zeta - AX(5)\frac{\zeta^2}{\mu}\frac{\partial\mu}{\partial\zeta}$$

$$+ AX(5)\frac{\zeta^2}{T}\frac{\partial T}{\partial\zeta} - AX(6)\zeta\frac{\partial G}{\partial\zeta} - AX(6)G$$

$$- AX(6)\frac{\zeta G}{\mu}\frac{\partial\mu}{\partial\zeta} + AX(6)\frac{\zeta G}{T}\frac{\partial T}{\partial\zeta} + AX(7)2G\frac{\partial G}{\partial\zeta}$$

$$+ AX(7)\frac{G^2}{\mu}\frac{\partial\mu}{\partial\zeta} - AX(7)\frac{G^2}{T}\frac{\partial T}{\partial\zeta} - AX(8)\frac{T}{\mu}\frac{\partial\mu}{\partial\zeta}\Bigg\}$$

$$\alpha_{\phi 4} = -AX(1)\frac{\mu\zeta}{\Phi^2 T}$$

$$\alpha_{\phi 5} = -AX(2)\frac{\mu G}{\Phi^2 T} \tag{21}$$

Equation (20) is cast into a standard form which is convenient for the numerical solution technique presented in Chapter III. The AX(I) coefficients in Equation (21) are functions of the body geometry and the

outer-edge conditions. Since many of them occur a number of times, their explicit forms are given later in this section.

The η-momentum equation transformed into the Crocco variables form is

$$\frac{\partial^2 G}{\partial \zeta^2} + \alpha_{G1} \frac{\partial G}{\partial \zeta} + \alpha_{G2} G + \alpha_{G3} + \alpha_{G4} \frac{\partial G}{\partial \xi} + \alpha_{G5} \frac{\partial G}{\partial \eta} = 0 \tag{22}$$

where

$$\alpha_{G1} = AX(5) \frac{\mu}{\phi^2 T} \zeta^2 + AX(6) \frac{\mu \zeta G}{\phi^2 T} - AX(7) \frac{\mu G^2}{\phi^2 T} + AX(8) \frac{\mu}{\phi^2}$$

$$\alpha_{G2} = -AX(10) \frac{\mu \zeta}{\phi^2 T} - AX(11) \frac{\mu G}{\phi^2 T}$$

$$\alpha_{G3} = AX(9) \frac{\mu \zeta^2}{\phi^2 T} - AX(12) \frac{\mu}{\phi^2}$$

$$\alpha_{G4} = - AX(1) \frac{\mu \zeta}{\phi^2 T}$$

$$\alpha_{G5} = - AX(2) \frac{\mu G}{\phi^2 T} \tag{23}$$

The Crocco variables form of the energy equation is

$$\frac{\partial^2 \theta}{\partial \zeta^2} + \alpha_{\theta 1} \frac{\partial \theta}{\partial \zeta} + \alpha_{\theta 2} \theta + \alpha_{\theta 3} + \alpha_{\theta 4} \frac{\partial \theta}{\partial \xi} + \alpha_{\theta 5} \frac{\partial \theta}{\partial \eta} = 0 \tag{24}$$

where

$$\alpha_{\theta 1} = \frac{(1-Pr)}{\phi}\frac{\partial \phi}{\partial \zeta} + AX(5)\frac{\mu Pr\zeta^2}{\phi^2 T} + AX(6)\frac{\mu Pr\zeta G}{\phi^2 T}$$

$$- AX(7)\frac{\mu PrG^2}{\phi^2 T} + AX(8)\frac{\mu Pr}{\phi^2}$$

$$\alpha_{\theta 2} = 0$$

$$\alpha_{\theta 3} = - AX(13)\left(1 + \frac{\zeta}{\phi}\frac{\partial \phi}{\partial \zeta}\right)$$

$$- AX(14)\left[\frac{G}{\phi}\frac{\partial G}{\partial \zeta}\frac{\partial \phi}{\partial \zeta} + G\frac{\partial^2 G}{\partial \zeta^2} + \left(\frac{\partial G}{\partial \zeta}\right)^2\right]$$

$$\alpha_{\theta 4} = - AX(1)\frac{\mu Pr\zeta}{\phi^2 T}$$

$$\alpha_{\theta 5} = - AX(2)\frac{\mu PrG}{\phi^2 T} \qquad (25)$$

Although the grouping of some of the η-momentum equation coefficients in Equation (23) is not unique, they have been formulated analogous to the coefficients for the ξ-momentum and energy equations, and the groupings presented have proven well-behaved in the solution of the equations.

It should be noted that in performing the Crocco transformation, the density was eliminated from the equations through the application of the equation of state. Additionally, the Prandtl number has been assumed to be constant. No assumptions have been made concerning the viscosity law, although a Sutherland viscosity law was used in all calculations

performed in this investigation.

The coefficients AX(1) through AX(14) are functions of only ξ and η, and not ζ. They are essentially made up of body geometry data and data concerning conditions along the outer edge of the boundary layer. Their explicit forms are

$$AX(1) = \frac{\gamma}{\gamma-1} \frac{u_e p Z^2}{h_1}$$

$$AX(2) = \frac{\gamma}{\gamma-1} \frac{v_e p Z^2}{h_2}$$

$$AX(3) = \frac{\gamma}{\gamma-1} \frac{Z}{h_1 h_2} \frac{\partial}{\partial \xi} \left(h_2 Z p u_e\right)$$

$$AX(4) = \frac{\gamma}{\gamma-1} \frac{Z}{h_1 h_2} \frac{\partial}{\partial \eta} \left(h_1 Z p v_e\right)$$

$$AX(5) = \frac{\gamma}{\gamma-1} \frac{p Z^2}{h_1} \frac{\partial u_e}{\partial \xi}$$

$$AX(6) = \frac{\gamma}{\gamma-1} \frac{v_e p Z^2}{h_2} \frac{\partial \ell n(u_e h_1)}{\partial \eta}$$

$$AX(7) = \frac{\gamma}{\gamma-1} \frac{v_e^2 p Z^2}{u_e h_1 h_2} \frac{\partial h_2}{\partial \xi}$$

$$AX(8) = \frac{Z^2}{h_1 u_e} \frac{\partial p}{\partial \xi}$$

$$AX(9) = \frac{\gamma}{\gamma-1} \frac{u_e^2 p Z^2}{v_e h_1 h_2} \frac{\partial h_1}{\partial \eta}$$

$$AX(10) = \frac{\gamma}{\gamma-1} \frac{u_e p Z^2}{h_1} \frac{\partial \ell n(v_e h_2)}{\partial \xi}$$

$$AX(11) = \frac{\gamma}{\gamma-1}\frac{pZ^2}{h_2}\frac{\partial v_e}{\partial n}$$

$$AX(12) = \frac{Z^2}{v_e h_2}\frac{\partial p}{\partial n}$$

$$AX(13) = (1-Pr)\frac{u_e^2}{He}$$

$$AX(14) = (1-Pr)\frac{v_e^2}{He} \tag{26}$$

In utilizing the results of calculations performed using the Crocco-variables form of the three-dimensional boundary-layer equations presented in this section, certain parameters are of interest from a physical standpoint. The coefficient of longitudinal skin friction may be obtained in the form

$$C_{f_\xi}\, Z\, \sqrt{Re} = 2\, u_e(\phi)_{\zeta=0} \tag{27}$$

where

$$C_{f_\xi} = \frac{\left(\frac{\bar{\mu}}{\bar{h}_3}\frac{\partial \bar{u}}{\partial \zeta}\right)_{\zeta=0}}{\frac{1}{2}\,\bar{\rho}_\infty\,\bar{u}_\infty^2}$$

The coefficient of lateral skin friction can be obtained as

$$C_{f_n}\, Z\, \sqrt{Re} = 2v_e \left(\phi\,\frac{\partial G}{\partial \zeta}\right)_{\zeta=0} \tag{28}$$

where

$$C_{f_\eta} = \frac{\left(\frac{\bar{\mu}}{\bar{h}_3}\frac{\partial \bar{v}}{\partial \zeta}\right)_{\zeta=0}}{\frac{1}{2}\bar{\rho}_\infty \bar{u}_\infty^2}$$

The Stanton number may be represented as

$$St_\infty Z\sqrt{Re} = \left[\frac{-\phi}{Pr\ He(1-\theta)} \cdot \frac{\partial T}{\partial \zeta}\right]_{\zeta=0} \tag{29}$$

where

$$St_\infty = \frac{\left(\frac{\bar{\mu}\bar{C}_p}{Pr\ \bar{h}_3}\frac{\partial \bar{T}}{\partial \zeta}\right)_{\zeta=0}}{\bar{\rho}_\infty \bar{u}_\infty (\bar{H}_\infty - \bar{H}_{\zeta=0})}$$

The distance normal to the surface may be determined from

$$\frac{\bar{y}\sqrt{Re}}{\bar{L}Z} = \int_0^\zeta \frac{\mu}{\phi}\, d\zeta \tag{30}$$

III. BOUNDARY CONDITIONS

The appropriate boundary conditions needed to solve the set composed of Equations (20), (22), and (24) depend on the nature of the equations. This matter has been considered in some detail by Raetz (11), Der and Raetz (15), and Wang (16). In considering the situation for a general point P in the boundary layer, the concept of zones of influence and dependence have been developed, as illustrated in Figure 4. The partial differential equations are of an elliptic nature in the ζ direction, and the conditions at point P affect, and are in turn affected, by the conditions along the entire line which is normal to the surface

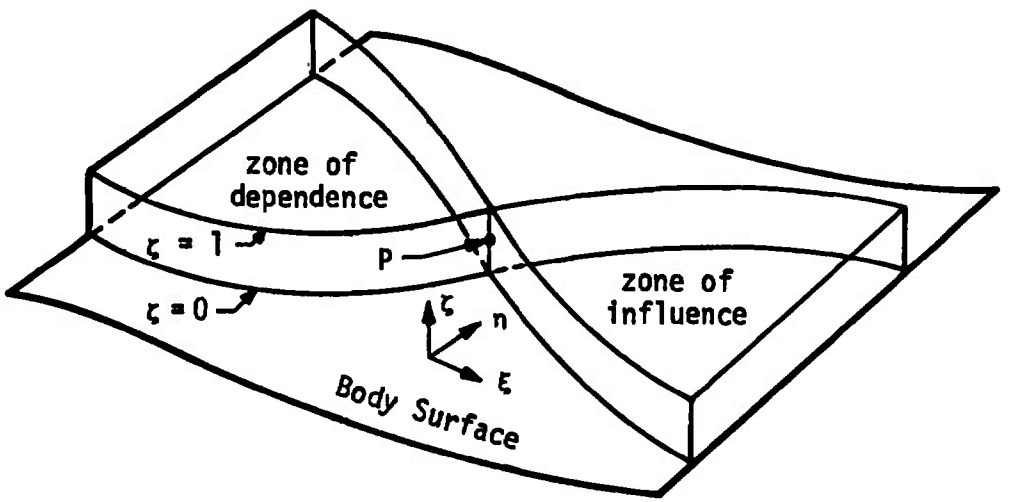

Figure 4. Zones of Influence and Dependence

from $\zeta = 0$ to $\zeta = 1$ and passes through P. This is a consequence of the diffusion phenomena which are involved. Downstream of P there is a zone of influence bounded by the surfaces $\zeta = 0$ and $\zeta = 1$ and by two surfaces called the "outer and inner characteristic envelopes". These characteristic envelopes are such that they are generated by the normals to the surface emanating from the projection on the surface of the streamlines having either the minimum or maximum angular displacement from the constant-η surfaces. The conditions at point P affect the conditions at all points within this zone of influence. Upstream of P there exists a similarly defined zone of dependence such that the conditions at P are dependent upon the conditions at all points within the zone of dependence.

The concept of dependence sub-zones associated with the governing equations is important in the determination of just what boundary data are required in order to solve the equations over a given region. The general characteristic surfaces of the governing equations are surfaces generated by straight lines normal to the body surface and extending from $\zeta = 0$ to $\zeta = 1$. If the solution is desired in a region bounded by the surfaces $\xi = \xi_1$, $\xi = \xi_2$, $\eta = \eta_1$, $\eta = \eta_2$, $\zeta = 0$, $\zeta = 1$, where $\xi_2 > \xi_1$ and $\eta_2 > \eta_1$, then the specification of data on the characteristic surfaces $\xi = \xi_1$, $\eta = \eta_1$, and $\eta = \eta_2$ is the maximum that could be required, in addition to data on $\zeta = 0$ and $\zeta = 1$. In fact, data are required on $\eta = \eta_1$ or $\eta = \eta_2$ only if there is flow across those surfaces and into the region under consideration. A given region may be divided into a number of sub-regions to provide convenient regions over which to

apply this concept.

In addition to indicating the appropriate boundary conditions needed to solve the boundary-layer equations, the concepts presented in this section are valuable in determining a proper numerical scheme for solving the equations, as will be indicated in this next chapter.

For the present problem of flow over a right circular cone, the governing equations degenerate to two-dimensional or even one-dimensional problems along the windward symmetry line and at the sharp tip, permitting the governing equations in these regions to be treated as simple boundary-value problems or as conventional two-dimensional parabolic systems, provided that appropriate boundary conditions are known at $\zeta = 0$ and $\zeta = 1$. These special similarity solutions, together with the boundary conditions for Φ, G, and θ on the surfaces $\zeta = 0$ and $\zeta = 1$, permit the solution of Equations (20), (22), and (24) over the entire surface of the body.

The boundary conditions to be imposed on G and θ at the body surface and at the outer edge of the boundary layer are the following:

at $\zeta = 0$:

$$G = 0$$

$$\theta = [\theta(\xi,\eta)]_{\zeta=0}, \text{ prescribed} \qquad (31)$$

at $\zeta = 1$:

$$G = 1$$

$$\theta = 1 \qquad (32)$$

The surface boundary condition on θ could also be a prescribed heat-transfer rate distribution, although that possibility is not treated in this investigation.

The surface boundary condition on Φ is obtained from evaluating Equation (19), the Crocco-variables form of the ξ-momentum equation, at $\zeta = 0$, where G is also zero. The resulting expression yields

$$\left(\frac{\partial \Phi}{\partial \zeta}\right)_{\zeta=0} = \left[\frac{\gamma}{\gamma-1}\,\frac{u_e\, pJ}{T} + AX(8)\,\frac{\mu}{\Phi}\right]_{\zeta=0} \tag{33}$$

The factor J in Equation (33) would be used to include surface mass transfer effects if transpiration or suction were being considered.

The outer-edge boundary condition on Φ may be obtained from the definition of Φ as

$$(\Phi)_{\zeta=1.0} = \left(\frac{\mu\, Z}{\sqrt{Re}\; u_e}\,\frac{du}{dy}\right)_{\zeta=1.0} \tag{34}$$

where

$$y = \frac{\overline{y}}{L}$$

In the classical treatment of boundary-layer theory, the term $(du/dy)_{\zeta=1.0}$ is set equal to zero. In the present treatment of the problem, however, where streamline swallowing is being considered, this term is equated to its value at a certain point in the inviscid flowfield. It should also be noted that u_e, v_e, and their variation with ξ and η must also be determined in an appropriate manner from the inviscid flowfield over the body. This matter is considered in the next section.

IV. TREATMENT OF STREAMLINE SWALLOWING

In this section the technique used to determine the boundary-layer outer-edge conditions through the treatment of the streamline-swallowing phenomenon is presented. Basically, the boundary-layer outer-edge conditions are determined on a surface in the inviscid flowfield which separates the flow entrained by the boundary layer from that not entrained by the boundary layer. The location of this inviscid separating surface is obtained by a mass balance between the boundary layer and the inviscid flowfield. In the actual computations the location of this surface is coupled to the solution of the boundary-layer equations, and is obtained in an iterative manner in conjunction with the solution of the boundary-layer equations. As noted previously, it is assumed that the boundary-layer displacement effects on the inviscid flowfield are negligible, and no such effects are considered in this investigation.

The description of the method of determining the location of the separating surface described in the previous paragraph is accomplished most easily by anticipating the finite-difference treatment used in the solution of the complete problem. The description of the method of determining the location of the inviscid separating surface is, therefore, done from a control-volume point of view which is analogous to the finite-difference treatment. Figure 5 shows a typical control volume for use in applying the mass-balance scheme. The control volume shown in Figure 5 represents either a rectangular parallelepiped region

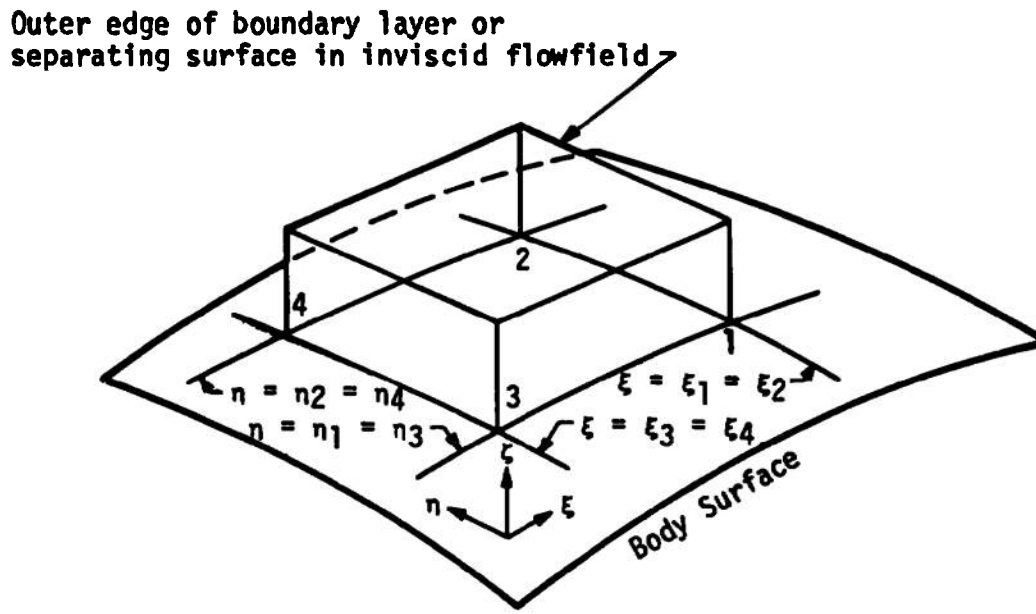

Figure 5. Control Volume for Streamline-Swallowing Mass Balance

of the boundary layer (in ξ, η, ζ coordinates), with its base on the body surface at $\zeta = 0$ and top at $\zeta = 1$, or a region in the inviscid flowfield having the same base, but with the top being in the inviscid separating surface.

The flow which crosses the indicated part of the inviscid separating surface is the same flow which is entrained by the boundary layer over the region with corners marked 1, 2, 3, and 4 in Figure 5. Let the sides of the control volume be denoted by the numbers at the corners of the base; let a prime superscript denote the boundary-layer flow through the control volume; and let an asterisk superscript denote the inviscid flow through the control volume. Letting $\dot{m}$ be the dimensional mass flow across a side of the control volume (typical explicit forms for $\dot{m}$ are presented shortly), and equating the mass flow across the top of the inviscid flow control volume to that across the top of the boundary-layer control volume yields

$$\dot{m}'_{3-4} + \dot{m}'_{1-3} - \dot{m}'_{2-4} - \dot{m}'_{1-2} = \dot{m}^*_{3-4} + \dot{m}^*_{1-3} - \dot{m}^*_{2-4} - \dot{m}^*_{1-2} \tag{35}$$

Were there surface mass transfer occurring, an additional term accounting for this would need to be added to Equation (35).

Typical forms for the $\dot{m}$ terms are presented in Equations (36) and (37); in the forms given the $\dot{m}$ are dimensional quantities, although, for simplicity, the bar over the symbol has been omitted.

$$\dot{m}'_{3-4} = \int_{\eta_3}^{\eta_4} \int_{0}^{1} \bar{\rho}\,\bar{u}\,\bar{h}_3\,d\zeta\,\bar{h}_2\,d\eta$$

$$\dot{m}'_{1-3} = \int_{\xi_3}^{\xi_1} \int_{0}^{1} \bar{\rho}\,\bar{v}\,\bar{h}_3\,d\zeta\,\bar{h}_1\,d\xi \qquad (36)$$

where $\bar{\rho}$, $\bar{u}$, and $\bar{v}$ refer to quantities in the boundary layer.

For the inviscid flow, typical forms are

$$\dot{m}^*_{3-4} = \int_{\eta_3}^{\eta_4} \int_{0}^{\bar{y}_{ss}} \bar{\rho}\,\bar{u}\,d\bar{y}\,\bar{h}_2\,d\eta$$

$$\dot{m}^*_{1-3} = \int_{\xi_3}^{\xi_1} \int_{0}^{\bar{y}_{ss}} \bar{\rho}\,\bar{v}\,d\bar{y}\,\bar{h}_1\,d\xi \qquad (37)$$

where $\bar{\rho}$, $\bar{u}$, and $\bar{v}$ here refer to quantities in the inviscid flowfield. The variable $\bar{y}$ is the dimensional distance normal to the body surface, and $\bar{y}_{ss}$ is the value of $\bar{y}$ on the inviscid separating surface along which the boundary-layer outer-edge conditions are taken.

In treating the problem of streamline swallowing by the boundary layer on a cone at angle of attack, Equation (35) is employed in an iteration scheme which results in determining $\bar{y}_{ss}$ (as a function of ξ and η) and the concomitant boundary-layer outer-edge conditions in a manner such that the final solution obtained for the boundary-layer equations

satisfies Equation (35). This iteration scheme is described in detail in the next chapter.

The inviscid flow field data required for the present problem were obtained using the numerical method of Jones (12) for treating the problem of steady supersonic inviscid flow around smooth conical bodies at incidence. This method has been shown to agree well with other theoretical methods and with experimental results, and it is very efficient in usage of computer time.

The inviscid flowfield over a conical body at incidence is itself conical. That is, flow properties are constant along any ray emanating from the apex of the body. This condition of conicity is used in Jones' method to reduce the problem to a set of elliptic non-linear partial differential equations in two independent variables. A transformation is introduced in which the unknown location of the shock wave becomes one of the boundaries, and the resulting equations are numerically solved by a very efficient numerical scheme. Limitations of the method are such that for cases of interest herein, solutions can be obtained for angles of attack up to a value approximately equal to the cone half-angle.

The variation in the shock wave strength from the windward side to the leeward side of a right circular cone at incidence is, of course, the origin of the streamline swallowing phenomenon. The inviscid flow-field associated with this problem is such that the entire body surface is wetted by fluid which crossed the most windward part of the bow shock. The fluid at some point off the body surface will have crossed

a weaker portion of the bow shock, and the fluid can be characterized by the entropy value it attains through crossing a particular part of the bow shock. In the neighborhood of the body surface the entropy, density, velocity, etc. (but not the pressure) change rapidly in the direction normal to the body surface, because of the bow shock wave strength variation. This region of large gradients in the direction normal to the body surface is generally referred to as the inviscid "entropy layer" because of its relation to the entropy change across the bow shock wave. This terminology will also be used in the discussion in this report. (The term "vortical layer", used by some authors, has the same meaning as the term entropy layer described above.)

CHAPTER III
NUMERICAL SOLUTION OF THE PROBLEM

The numerical scheme used to solve the coupled nonlinear second-order partial-differential Equations (20), (22), and (24), and the method used to determine the outer-edge boundary conditions through the streamline-swallowing treatment are presented in this chapter for the case of flow over a right circular cone at angle of attack. Basically, Equations (20), (22), and (24) are replaced by a set of consistent linearized algebraic equations. This set is of tridiagonal form and is solved by means of an especially efficient algorithm. The finite-difference scheme is an implicit one, chosen because of the lack of problems with stability and mesh size, as opposed to explicit schemes.

For those situations involving derivatives with respect to ξ or η, the finite-difference formulation follows that introduced by Crank and Nicholson (17) or the three-dimensional analogue of this form, as used by Dwyer (18). The set of finite-difference equations so developed is uniformly valid to second-order in the mesh spacings of the finite-difference grid. The α-terms given in Equations (21), (23), and (25) are generally assumed to be known, resulting in the uncoupling and linearization of the set of equations which must be solved. This assumption is removed by an "updating" of the α-terms through iteration on the solution of the set of finite-difference equations. In addition to this iteration, there is a second iteration involved in determining the outer-edge

conditions through the mass-balance treatment of the streamline-swallowing phenomenon. Figure 6 shows a simplified flow diagram of the digital computer program used to solve the finite-difference equations at a general point on the body. (All computations made in this investigation were performed on a Control Data Corporation Model 1604B digital computer.)

At this point the explicit form of the coordinate system and the metric coefficients used will be described, with reference to Figure 7. Letting ξ be along rays of the cone, with $\xi = 0$ at the apex, and η be the angular displacement about the cone axis from the windward plane of symmetry, and defining $\bar{h}_1$ to be equal to the reference length $\bar{L}$, the following results may be obtained:

$$h_1 = 1.0$$

$$h_2 = \xi \sin \theta_c \tag{38}$$

Examination of the AX coefficients given in Equations (26) shows that the term Z^2/h_2 occurs a number of times. At the apex of the cone $h_2 = 0$; however, defining Z as

$$Z = \sqrt{\xi} \tag{39}$$

gives $\frac{Z^2}{h_2} = \frac{1}{\sin \theta_c}$, and this term is well defined everywhere.

Although the boundary-layer equations are not physically applicable at the apex of a cone, they are mathematically amenable to solution there, and the solution so obtained may be considered applicable

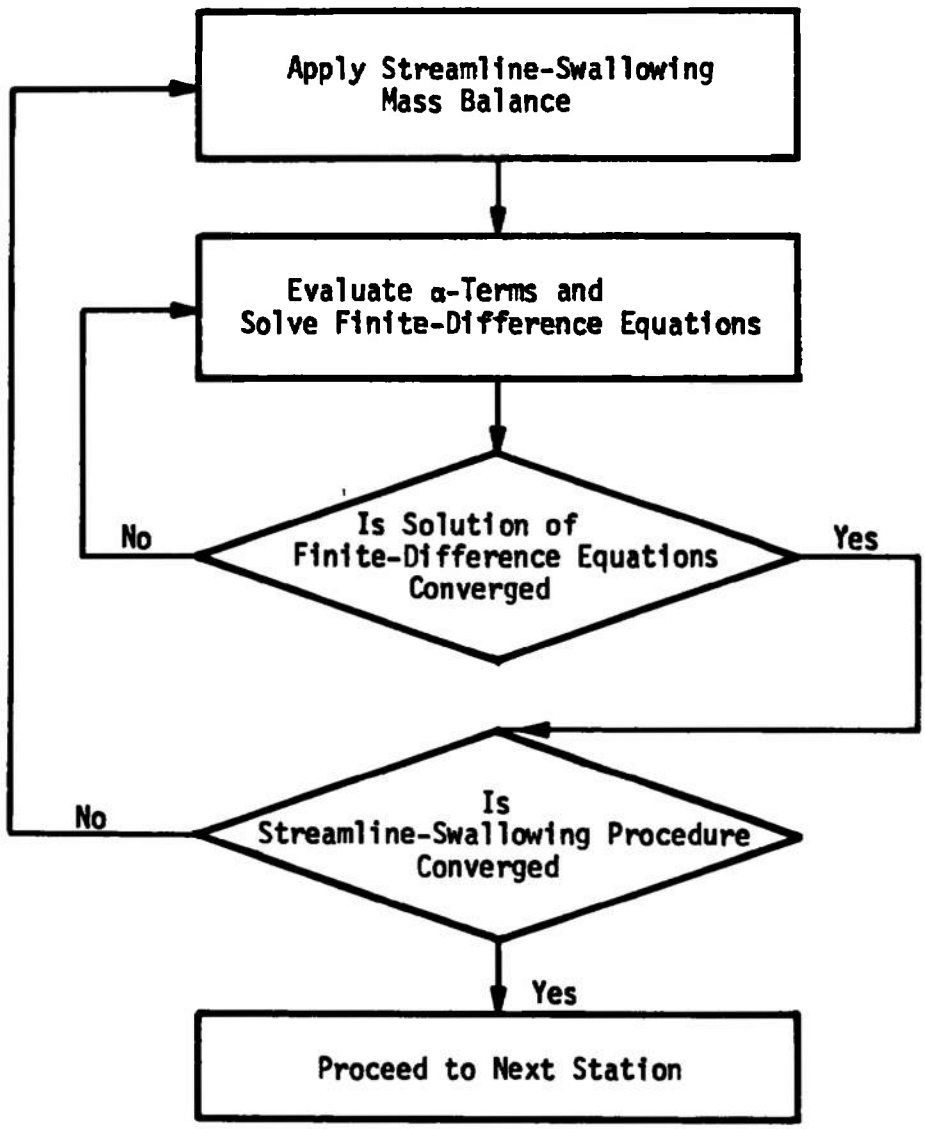

Figure 6. Simplified Flow Diagram for Solution at a General ξ - η Station

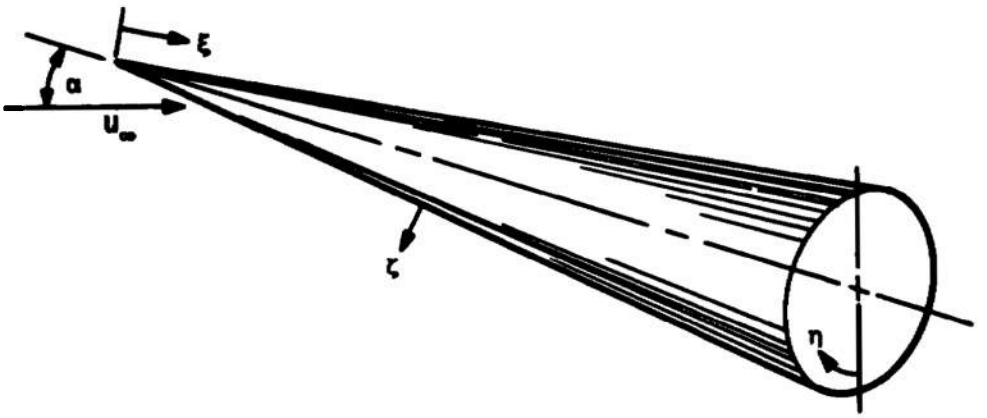

Figure 7. Coordinate System for Right Circular Cone

"near" the apex. At $\xi = 0$, $\eta = 0$, where $\eta = 0$, $\zeta = 0$ coincides with the windward-most ray of the body, the governing equations reduce to a two-point boundary-value problem dependent only upon ζ. For $\xi = 0$, $\eta > 0$, the equations have no ξ-dependence, and the solution may be obtained by beginning with the solution obtained at $\eta = 0$ and "marching" around the body. For the surface $\eta = 0$, $\xi > 0$, streamline-swallowing effects on the solution of the boundary-layer equations must be minimal, and in this investigation the similarity solution obtained at $\eta = 0$, $\xi = 0$ has been assumed to apply along $\eta = 0$, $\xi > 0$ even when streamline-swallowing is being considered over the region $\xi > 0$, $\eta > 0$.

So long as the lateral velocity component is greater than or equal to zero, the similarity solutions along the surface $\xi = 0$ and the surface $\eta = 0$, together with the boundary conditions on $\zeta = 0$ and $\zeta = 1$, provide sufficient data to allow the solution of the governing equations over the region $0 < \eta < \pi$, $\xi > 0$, in keeping with the discussion in Section III of Chapter II.

The following sections describe the method of solution used for the governing equations (a) at $\xi = 0$, $\eta = 0$, (b) along $\xi = 0$, $\eta > 0$, and (c) for $\xi > 0$, $\eta > 0$, and the final section of this chapter describes the treatment of the streamline-swallowing phenomenon through the application of the mass-balance scheme described in the previous chapter.

I. SOLUTION AT $\xi = 0$ AND $\eta = 0$

At $\xi = 0$, $\eta = 0$, the AX coefficients which are not identically zero are the following:

$$AX(3) = \frac{\gamma}{\gamma-1} \frac{3}{2} pu_e$$

$$AX(4) = \frac{\gamma}{\gamma-1} \frac{p}{\sin \theta_c} \frac{\partial v_e}{\partial \eta}$$

$$AX(10) = \frac{\gamma}{\gamma-1} pu_e$$

$$AX(11) = \frac{\gamma}{\gamma-1} \frac{p}{\sin \theta_c} \frac{\partial v_e}{\partial \eta}$$

$$AX(12) = \frac{1}{v_e \sin \theta_c} \frac{\partial p}{\partial \eta} = \frac{1}{\sin \theta_c} \left(\frac{\partial v_e}{\partial \eta} \right)^{-1} \frac{\partial^2 p}{\partial \eta^2}$$

$$AX(13) = (1-Pr) \frac{u_e^2}{He} \tag{40}$$

In obtaining these forms, the symmetry (with respect to η) of u_e and p at $\eta = 0$ were used, together with $\partial p/\partial \xi = 0$ and $v_e = 0$. Additionally, it has been assumed that, in the vicinity of $\eta = 0$, u_e and v_e are functions of only η. This is consistent with the conical flow and the assumption that streamline-swallowing effects are negligible along $\eta = 0$. The indeterminate form of AX(12) may be conveniently evaluated by L'Hospital's rule, as the second form shows.

The introduction of the AX coefficients for $\xi = 0$, $\eta = 0$ into Equations (20) through (25) yields the following general form for the governing equations at $\xi = 0$, $\eta = 0$, where X represents Φ, G, or θ.

$$\frac{\partial^2 X}{\partial \zeta^2} + \alpha_{X1} \frac{\partial X}{\partial \zeta} + \alpha_{X2} X + \alpha_{X3} = 0 \tag{41}$$

The required α-terms take the following forms:

$$\alpha_{\phi 1} = 0$$

$$\alpha_{\phi 2} = 0$$

$$\alpha_{\phi 3} = \frac{\mu}{\phi T} \left\{ AX(3)\zeta + AX(4)G \right\}$$

$$\alpha_{G1} = 0$$

$$\alpha_{G2} = - \frac{\mu}{\phi^2 T} \left\{ AX(10)\zeta + AX(11)G \right\}$$

$$\alpha_{G3} = - AX(12) \frac{\mu}{\phi^2}$$

$$\alpha_{\theta 1} = \frac{1-Pr}{\phi} \frac{\partial \phi}{\partial \zeta}$$

$$\alpha_{\theta 2} = 0$$

$$\alpha_{\theta 3} = - AX(13) \left\{ 1 + \frac{\zeta}{\phi} \frac{\partial \phi}{\partial \zeta} \right\} \qquad (42)$$

The α-terms omitted from the set of Equations (42) are identically zero. The set of equations represented by Equation (41) is a set of coupled, nonlinear, second-order ordinary differential equations with independent variable ζ.

For the case of $\eta = 0$, $\xi > 0$, Equation (41) must have added to it the term $\alpha_{X4} \frac{\partial X}{\partial \xi}$, and except for the addition of the α_{X4}-terms, Equations (42) remain unchanged. If the boundary conditions on ϕ, G, and

θ (at $\zeta = 0$ and $\zeta = 1.0$) and the edge conditions u_e, v_e, etc. are not functions of ξ, then the solution obtained for the set represented by Equation (41) at $\xi = 0$, $\eta = 0$ is also the applicable solution for $\xi > 0$, $\eta = 0$. The conditions necessary for these similarity solutions to be valid are (in addition to the previous assumption of u_e and v_e being functions of only η near $\eta = 0$) that the surface temperature not be a function of ξ and that $J = wZ/u_e$ not be a function of ξ. With $Z = \sqrt{\xi}$, this latter condition is equivalent to requiring that any surface mass transfer velocity be proportional to the inverse of the square root of ξ along any ray of the cone. These two conditions are met in this investigation by having zero mass transfer and a constant surface temperature.

In order to cast Equation (41) into an appropriate finite-difference form, a grid is established which divides the region from $\zeta = 0$ to $\zeta = 1$ into NZ - 1 equal increments with NZ grid points. At each interior point finite-difference forms for the first and second derivatives with respect to ζ are obtained from Taylor series truncation as

$$\left(\frac{\partial X}{\partial \zeta}\right)_n = \frac{X_{n+1} - X_{n-1}}{2\,\Delta\zeta} + O(\Delta\zeta^2)$$

$$\left(\frac{\partial^2 X}{\partial \zeta^2}\right)_n = \frac{X_{n+1} - 2X_n + X_{n-1}}{\Delta\zeta^2} + O(\Delta\zeta^2) \tag{43}$$

where $\Delta\zeta = \frac{1}{NZ-1}$, and $O(\Delta\zeta^2)$ means that the lowest order terms which have been neglected in the Taylor series development are of the form $\Delta\zeta^2$ times some quantity which is independent of $\Delta\zeta$. The subscript n refers to the grid point under consideration, where n = 1 refers to $\zeta = 0$ and n = NZ refers to $\zeta = 1$.

The resulting finite-difference equivalent of Equation (41) is

$$X_n = A_{X,n}\, X_{n+1} + B_{X,n}\, X_{n-1} + C_{X,n} \tag{44}$$

The explicit forms of A, B, and C are

$$A_{X,n} = \frac{2 + \alpha_{X1,n}\,\Delta\zeta}{2(2-\alpha_{X2,n}\,\Delta\zeta^2)}$$

$$B_{X,n} = \frac{2 - \alpha_{X1,n}\,\Delta\zeta}{2(2 -\alpha_{X2,n}\,\Delta\zeta^2)}$$

$$C_{X,n} = \frac{\alpha_{X3,n}\,\Delta\zeta^2}{2-\alpha_{X2,n}\,\Delta\zeta^2} \tag{45}$$

In the evaluation of the finite-difference forms of the α-terms, all of the quantities involved are taken from an initial approximation or the previous iteration, and may, therefore, be considered known. The quantities involved in the derivatives in Equation (41) are treated as unknowns and ultimately appear as the unknowns in Equation (44).

An equation of the form of Equation (44) is written for each value of n between 1 and NZ, assuming that Φ, G, and θ are known at $\zeta = 0$ and $\zeta = 1$; however, for $n = 2$ the coefficients so determined for the Φ equation must be modified to take into account the surface boundary condition on Φ as given by Equation (33). For zero surface mass transfer and $\partial p/\partial\xi = 0$, as in a conical flow, the boundary condition reduces to

$$\left(\frac{\partial\Phi}{\partial\zeta}\right)_{\zeta=0} = 0 \tag{46}$$

Applying a finite-difference relation of $O(\Delta\zeta^2)$ accuracy to Equation (46) yields

$$\Phi_1 = \frac{4}{3}\Phi_2 - \frac{1}{3}\Phi_3 \tag{47}$$

where the subscripts represent the grid locations, with the subscript "1" being the node on the surface. From Equation (44)

$$\Phi_2 = A^+_{\Phi,2}\,\Phi_3 + B^+_{\Phi,2}\,\Phi_1 + C^+_{\Phi,2} \tag{48}$$

where the plus superscripts refer to forms obtained assuming Φ_1 to be known. Eliminating Φ_1 from Equations (47) and (48) yields the coefficients which may be applied to take into account the surface derivative boundary condition on Φ

$$A_{\Phi,2} = \frac{A^+_{\Phi,2} - \frac{B^+_{\Phi,2}}{3}}{1 - \frac{4}{3}B^+_{\Phi,2}}$$

$$B_{\Phi,2} = 0$$

$$C_{\Phi,2} = \frac{C^+_{\Phi,2}}{1 - \frac{4}{3}B^+_{\Phi,2}} \tag{49}$$

At $\xi = 0$, $\eta = 0$, it is assumed that $(\Phi)_{\zeta=1} = 0$. The boundary conditions on G and θ are those given in Equations (31) and (32). With the introduction of Equations (49) and the boundary conditions just mentioned the three sets of equations represented by Equation (44) may be solved for the values of Φ, G, and θ for $2 \leq n \leq NZ-1$. The value of Φ_1

can be determined from Equation (47) after the values of Φ_2 and Φ_3 are found.

The solution of the three sets of equations of the form of Equation (44) was performed by the standard methods for linear tridiagonal algebraic systems. The particular form of Equation (44) is that used by Patankar and Spalding (19), and it has the advantage of requiring less computer storage than forms which involve four coefficient terms rather than three. Knowing the values of the dependent variables at n = 1 and n = NZ (corresponding to $\zeta = 0$ and $\zeta = 1$, respectively) except for Φ_1, which need not be known, according to the treatment given previously, each of the sets of equations represented by Equation (44) may be solved for X_2 through X_{NZ-1} by applying

$$X_n = P_n X_{n+1} + Q_n$$

where

$$P_n = \frac{A_{X,n}}{1 - B_{X,n} P_{n-1}}$$

$$Q_n = \frac{B_{X,n} Q_{n-1} + C_{X,n}}{1 - B_{X,n} P_{n-1}}$$

with

$$P_2 = A_{X,2}$$

$$Q_2 = B_{X,2} X_1 + C_2 \qquad (50)$$

The set of P's and Q's can be determined consecutively from n = 2 through n = NZ-1, and the set of values of X_n may be determined beginning with

$n = NZ - 1$ and proceeding to $n = 2$. The procedure indicated by Equations (50) may be considered a special case of the Gaussian elimination procedure.

After solving the equations represented by Equation (44), the α terms are recomputed, using the results of the solution, and the equations are solved again. This procedure is repeated until the solution converges, i.e., until the difference between successive solutions is sufficiently small.

The determination of the outer-edge conditions needed in the AX coefficients, i.e., u_e, v_e, $\partial v_e/\partial n$, etc., will now be discussed. Generally speaking, taking these data to be those corresponding to the inviscid surface data is equivalent to the classical treatment of the problem and neglects any effect of streamline swallowing. Such classical solutions were obtained in this investigation for comparison with solutions which included the effects of streamline swallowing. With respect to the location $\xi = 0$, $\eta = 0$, the edge conditions could be taken from any point in the inviscid flow on the normal to the surface between the surface and the shock wave, regardless of considerations of streamline swallowing, without significantly affecting the computed boundary-layer data. When considering the situation near $\eta = \pi$, where streamline-swallowing effects were found to be more significant, it was necessary for stability reasons that at $\xi = 0$ the outer-edge conditions be taken at some location in the inviscid flowfield out of the region near the surface where large gradients (with respect to the direction normal to the surface) existed in the inviscid flowfield data. Therefore, for the sake of consistency,

when streamline swallowing was being considered, all of the outer-edge conditions at $\xi = 0$, including those at $\eta = 0$ were taken at a location in the inviscid flowfield off the body surface. The exact location from which these data were taken had no significant effect on the solutions obtained for values of ξ outside the neighborhood of $\xi = 0$.

II. SOLUTION AT $\xi = 0$ AND $\eta > 0$

Having obtained the solution at $\xi = 0$, $\eta = 0$, the solution to the governing equations may be obtained at successively greater values of η by "marching" around the body, provided that v is not less than zero. If the outer-edge conditions are taken to be the inviscid surface data, then the solutions obtained are the classical similarity solutions.

For $\xi = 0$, $\eta > 0$, the AX coefficients have the following forms:

$$AX(1) = 0$$

$$AX(2) = \frac{\gamma}{\gamma-1} \frac{v_e\, p}{\sin \theta_c}$$

$$AX(3) = \frac{\gamma}{\gamma-1} \frac{3}{2} p u_e$$

$$AX(4) = \frac{\gamma}{\gamma-1} \frac{1}{\sin \theta_c} \left(p \frac{\partial v_e}{\partial \eta} + v_e \frac{\partial p}{\partial \eta} \right)$$

$$AX(5) = 0$$

$$AX(6) = \frac{\gamma}{\gamma-1} \frac{v_e\, p}{\sin \theta_c} \frac{1}{u_e} \frac{\partial u_e}{\partial \eta}$$

$$AX(7) = \frac{\gamma}{\gamma-1} \frac{v_e^2 \, p}{u_e}$$

$$AX(8) = 0$$

$$AX(9) = 0$$

$$AX(10) = \frac{\gamma}{\gamma-1} pu_e$$

$$AX(11) = \frac{\gamma}{\gamma-1} \frac{p}{\sin \theta_c} \frac{\partial v_e}{\partial \eta}$$

$$AX(12) = \frac{1}{v_e \sin \theta_c} \frac{\partial p}{\partial \eta}$$

$$AX(13) = (1-Pr) \frac{u_e^2}{He}$$

$$AX(14) = (1-Pr) \frac{v_e^2}{He} \qquad (51)$$

The introduction of Equations (51) into Equations (20) through (25) yields the following general form for the governing equations for $\xi = 0$, $\eta > 0$:

$$\frac{\partial^2 X}{\partial \zeta^2} + \alpha_{X1} \frac{\partial X}{\partial \zeta} + \alpha_{X2} X + \alpha_{X3} + \alpha_{X5} \frac{\partial X}{\partial \eta} = 0 \qquad (52)$$

where X represents ϕ, G, or θ.

The required α-terms have the following forms:

$$\alpha_{\phi 1} = \frac{\mu G}{\phi^2 T} \left\{ AX(6)\zeta - AX(7)G \right\}$$

$$\alpha_{\phi 2} = 0$$

$$\alpha_{\phi 3} = \frac{\mu}{\phi T}\left\{AX(2)\left[\frac{\partial G}{\partial \eta} + \frac{G}{\mu}\frac{\partial \mu}{\partial \eta} - \frac{G}{T}\frac{\partial T}{\partial \eta}\right] + AX(3)\zeta + AX(4)G\right.$$

$$\left. + AX(6)\left[-\zeta\frac{\partial G}{\partial \zeta} - G - \frac{\zeta G}{\mu}\frac{\partial \mu}{\partial \zeta} + \frac{\zeta G}{T}\frac{\partial T}{\partial \zeta}\right] + AX(7)\left[2G\frac{\partial G}{\partial \zeta} + \frac{G^2}{\mu}\frac{\partial \mu}{\partial \zeta} - \frac{G^2}{T}\frac{\partial T}{\partial \zeta}\right]\right\}$$

$$\alpha_{\phi 5} = -AX(2)\frac{\mu G}{\phi^2 T}$$

$$\alpha_{G1} = \alpha_{\phi 1}$$

$$\alpha_{G2} = \frac{\mu}{\phi^2 T}\left\{-AX(10)\zeta - AX(11)G\right\}$$

$$\alpha_{G3} = -AX(12)\frac{\mu}{\phi^2}$$

$$\alpha_{G5} = \alpha_{\phi 5}$$

$$\alpha_{\theta 1} = \alpha_{\phi 1}\,Pr + \frac{(1-Pr)}{\phi}\frac{\partial \phi}{\partial \zeta}$$

$$\alpha_{\theta 2} = 0$$

$$\alpha_{\theta 3} = -AX(13)\left(1 + \frac{\zeta}{\phi}\frac{\partial \phi}{\partial \zeta}\right) - AX(14)\left\{\frac{G}{\phi}\frac{\partial G}{\partial \zeta}\frac{\partial \phi}{\partial \zeta} + G\frac{\partial^2 G}{\partial \zeta^2} + \left(\frac{\partial G}{\partial \zeta}\right)^2\right\}$$

$$\alpha_{\theta 5} = \alpha_{\phi 5}\,Pr \qquad (53)$$

The solution to the set of equations represented by Equation (52) for $\xi = 0$, $\eta > 0$ are the similarity solutions (with respect to ξ), provided that the edge conditions do not vary with ξ, the surface temperture is not a function of ξ, and any surface mass transfer velocity varies as the inverse of the square root of ξ.

In order to numerically treat Equation (52), a finite-difference grid is established over the region $\xi = 0$, $0 < \eta \leq \pi$, $0 \leq \zeta \leq 1$. The grid employs uniform step-sizes in both the η and ζ directions, although a constant step-size in only ζ is required for the finite-difference scheme used. The scheme which is used employs the known results at a given value of η in determining the solution at the succeeding η-grid location. If the solution is known at the typical η-location indicated by the subscript i=1 and is to be found at the η-location indicated by i=2, where $X_{i,j}$ indicates the value of the variable X at the η-location i and the ζ-grid location j, then the finite-difference expressions required to cast Equation (52) into finite-difference form at the point (0,n) indicated in Figure 8 are the following:

$$X_{0,n} = \frac{X_{1,n} + X_{2,n}}{2} + O(\Delta^2)$$

$$\left(\frac{\partial X}{\partial \eta}\right)_{0,n} = \frac{X_{2,n} - X_{1,n}}{\Delta \eta} + O(\Delta^2)$$

$$\left(\frac{\partial X}{\partial \zeta}\right)_{0,n} = \frac{X_{1,n+1} - X_{1,n-1} + X_{2,n+1} - X_{2,n-1}}{4\Delta\zeta} + \eta(\Delta^2)$$

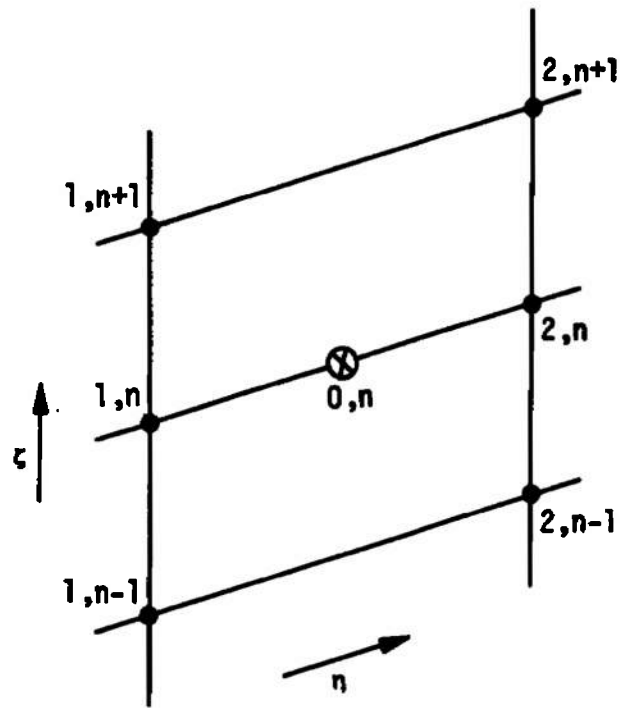

Figure 8. Typical Section of Finite-Difference Grid for $\xi = 0$, $\eta > 0$

$$\left(\frac{\partial^2 X}{\partial \zeta^2}\right)_{0,n} = \frac{X_{1,n+1} - 2X_{1,n} + X_{1,n-1} + X_{2,n+1} - 2X_{2,n} + X_{2,n-1}}{2\Delta\zeta^2}$$

$$+ O(\Delta^2) \tag{54}$$

where $\Delta\zeta$ is as described in the previous section, $\Delta\eta = \frac{\pi}{NETA-1}$, and NETA-1 is the number of η-increments between $\eta = 0$ and $\eta = \pi$. In Equation (54), $O(\Delta^2)$ implies that the lowest order terms neglected are of the form of a second-order term in $\Delta\xi$ or $\Delta\eta$ times some quantity which is independent of the mesh spacing. The forms given in Equations (54) are consistent with those of Crank and Nicholson (17), and their introduction into Equation (52) yields the following general form for the corresponding finite-difference equation

$$X_{2,n} = A_{X,n}X_{2,n+1} + B_{X,n}X_{2,n-1} + C_{X,n} \tag{55}$$

where A, B, and C are evaluated at (0,n). The explicit forms of A, B, and C are

$$A_{X,n} = \frac{\frac{1}{2\Delta\zeta^2} + \frac{\alpha_{X1}}{4\Delta\zeta}}{\frac{1}{\Delta\zeta^2} - \frac{\alpha_{X2}}{2} - \frac{\alpha_{X5}}{\Delta\eta}}, \quad B_{X,n} = \frac{\frac{1}{2\Delta\zeta^2} - \frac{\alpha_{X1}}{4\Delta\zeta}}{\frac{1}{\Delta\zeta^2} - \frac{\alpha_{X2}}{2} - \frac{\alpha_{X5}}{\Delta\eta}}$$

$$C_{X,n} = \frac{1}{\frac{1}{\Delta\zeta^2} - \frac{\alpha_{X2}}{2} - \frac{\alpha_{X5}}{\Delta\eta}} \left\{ X_{1,n}\left(\frac{\alpha_{X2}}{2} - \frac{\alpha_{X5}}{\Delta\eta} - \frac{1}{\Delta\zeta^2}\right) \right.$$

$$\left. + X_{1,n-1}\left(\frac{1}{2\Delta\zeta^2} - \frac{\alpha_{X1}}{4\Delta\zeta}\right) + X_{1,n+1}\left(\frac{1}{2\Delta\zeta^2} + \frac{\alpha_{X1}}{4\Delta\zeta}\right) + \alpha_{X3} \right\} \tag{56}$$

For X equal to each of Φ, G, and θ an equation of the form of Equation (55) can be written for $1 < n < NZ$, where the surface boundary condition of Φ is treated as described in the previous section. The treatment of the outer-edge data required for the AX coefficients, which are evaluated at $\eta = \frac{\eta 1 + \eta 2}{2}$, is also as described in the previous section. The α terms in Equations (56) are evaluated at the point (0,n) using the forms given in Equations (54).

All of the data required in the α terms are treated as known, using initial approximations or results from the previous iteration. Thus, the three sets of equations represented by Equation (55) can be solved by application of Equations (50). The iteration scheme previously described is used to eliminate the assumption made concerning the α terms. Using the solution obtained at $\xi = 0$, $\eta = 0$ as the initial known set of data, the solution method may be applied at consecutively increasing values of η, with each solution obtained providing the known solution for the next step.

The boundary conditions and outer-edge data required for $\xi = 0$, $\eta > 0$ have been treated as described in the previous section, including obtaining the classical similarity solutions by using the inviscid surface data for outer-edge conditions.

III. SOLUTION FOR $\xi > 0$ AND $\eta > 0$

Having the solution to the finite-difference forms of the governing equations for $\xi = 0$, $\eta = 0$ (which are also used as similarity solutions along $\xi > 0, \eta = 0$) and for $\xi = 0$, $\eta > 0$, the solution of the

problem for the region $\xi > 0$, $\eta > 0$ is obtained using a finite-difference formulation which is the three-dimensional analogue of the Crank-Nicholson scheme. This treatment is valid for non-negative values of v. For cases with v less than zero the scheme violates the influence principal of Raetz in that the flow history convected by the negative v would not be properly considered. Krause (20) has considered the problem of negative v from a stability viewpoint and has suggested a finite-difference scheme which would be stable for negative values of the lateral velocity component. Krause's method has not been used in this investigation because it would have application only very near the leeward-most ray of a cone at relatively large angles-of-attack, and that situation is not of primary interest.

For $\xi > 0$, $\eta > 0$, the AX coefficients have the following forms:

$$AX(1) = \frac{\gamma}{\gamma-1} \rho u_e \xi$$

$$AX(2) = \frac{\gamma}{\gamma-1} \frac{v_e \rho}{\sin \theta_c}$$

$$AX(3) = \frac{\gamma}{\gamma-1} \rho \left(\frac{3}{2} u_e + \frac{\xi \partial u_e}{\partial \xi} \right)$$

$$AX(4) = \frac{\gamma}{\gamma-1} \frac{1}{\sin \theta_c} \left(\rho \frac{\partial v_e}{\partial \eta} + v_e \frac{\partial p}{\partial \eta} \right)$$

$$AX(5) = \frac{\gamma}{\gamma-1} \rho \xi \frac{\partial u_e}{\partial \xi}$$

$$AX(6) = \frac{\gamma}{\gamma-1} \frac{v_e \rho}{\sin \theta_c} \frac{1}{u_e} \frac{\partial u_e}{\partial \eta}$$

$$AX(7) = \frac{\gamma}{\gamma-1} \frac{v_e^2 \, p}{u_e}$$

$$AX(8) = 0$$

$$AX(9) = 0$$

$$AX(10) = \frac{\gamma}{\gamma-1} \left(u_e p + \frac{u_e p \xi}{v_e} \frac{\partial v_e}{\partial \xi} \right)$$

$$AX(11) = \frac{\gamma}{\gamma-1} \frac{p}{\sin \theta_c} \frac{\partial v_e}{\partial \eta}$$

$$AX(12) = \frac{1}{v_e \sin \theta_c} \frac{\partial p}{\partial \eta}$$

$$AX(13) = (1-Pr) \frac{u_e^2}{He}$$

$$AX(14) = (1-Pr) \frac{v_e^2}{He} \tag{57}$$

The general form of the governing equations for $\xi > 0$, $\eta > 0$ is

$$\frac{\partial^2 X}{\partial \zeta^2} + \alpha_{X1} \frac{\partial X}{\partial \zeta} + \alpha_{X2} X + \alpha_{X3} + \alpha_{X4} \frac{\partial X}{\partial \xi} + \alpha_{X5} \frac{\partial X}{\partial \eta} = 0 \tag{58}$$

where

$$\alpha_{\Phi 1} = \frac{\mu}{\Phi^2 T} \left\{ AX(5)\zeta^2 + AX(6)\zeta G - AX(7)G^2 + AX(8)T \right\}$$

$$\alpha_{\Phi 2} = 0$$

$$\alpha_{\phi 3} = \frac{\mu}{\phi T}\left\{ AX(1)\left[\frac{\zeta}{\mu}\frac{\partial \mu}{\partial \xi} - \frac{\zeta}{T}\frac{\partial T}{\partial \xi}\right] + AX(2)\left[\frac{\partial G}{\partial \eta} + \frac{G}{\mu}\frac{\partial \mu}{\partial \eta} - \frac{G}{T}\frac{\partial T}{\partial \eta}\right] + AX(3)\zeta + AX(4)G + AX(5)\left[-2\zeta\frac{\zeta^2}{\mu}\frac{\partial \mu}{\partial \zeta} + \frac{\zeta^2}{T}\frac{\partial T}{\partial \zeta}\right] + AX(6)\left[-\frac{\zeta \partial G}{\partial \zeta} - G - \frac{\zeta G}{\mu}\frac{\partial \mu}{\partial \zeta} + \frac{\zeta G}{T}\frac{\partial T}{\partial \zeta}\right] + AX(7)\left[2G\frac{\partial G}{\partial \zeta} + \frac{G^2}{\mu}\frac{\partial \mu}{\partial \zeta} - \frac{G^2}{T}\frac{\partial T}{\partial \zeta}\right] - AX(8)\frac{T}{\mu}\frac{\partial \mu}{\partial \zeta}\right\}$$

$$\alpha_{\phi 4} = - AX(1)\frac{\mu\zeta}{\phi^2 T}$$

$$\alpha_{\phi 5} = - AX(2)\frac{\mu G}{\phi^2 T}$$

$$\alpha_{G1} = \alpha_{\phi 1}$$

$$\alpha_{G2} = \frac{\mu}{\phi^2 T}\left\{ - AX(10)\zeta - AX(11)G\right\}$$

$$\alpha_{G3} = \frac{\mu}{\phi^2 T}\left\{ AX(8)\zeta^2 - AX(12)T\right\}$$

$$\alpha_{G4} = \alpha_{\phi 4}$$

$$\alpha_{G5} = \alpha_{\phi_5}$$

$$\alpha_{\theta 1} = \alpha_{\phi_1} \, Pr + \frac{(1-Pr)}{\phi} \frac{\partial \phi}{\partial \zeta}$$

$$\alpha_{\theta 2} = 0$$

$$\alpha_{\theta 3} = - AX(13) \left(1 + \frac{\zeta}{\phi} \frac{\partial \phi}{\partial \zeta} \right) - AX(14) \left[\frac{G}{\phi} \frac{\partial G}{\partial \zeta} \frac{\partial \phi}{\partial \zeta} + G \frac{\partial^2 G}{\partial \zeta^2} + \left(\frac{\partial G}{\partial \zeta} \right)^2 \right]$$

$$\alpha_{\theta 4} = \alpha_{\phi 4} \, Pr$$

$$\alpha_{\theta 5} = \alpha_{\phi 5} \, Pr \qquad (59)$$

The finite-difference grid used for $\xi > 0$, $\eta > 0$ is indicated in Figure 9. Considering the general grid point (i,j),i = 1, 3, and 4 represent points where solutions have previously been obtained, while the solution is to be determined at i=2. The basic approach is that initially i=3 and 4 represent locations where $\xi = 0$, for which solutions have been obtained as described in the two previous sections. The locations represented by i=1 and 3 are initially at $\eta = 0$, where data are known from the similarity solutions employed there. For a given value of ξ, solutions are obtained at consecutive values of η by marching from $\eta = 0$ toward $\eta = \pi$. After having obtained solutions as far as desired in η, ξ is incremented and the procedure is repeated.

The basic finite-difference expressions needed to cast Equation (58) into finite-difference form at the point (0,n) shown in Figure 9

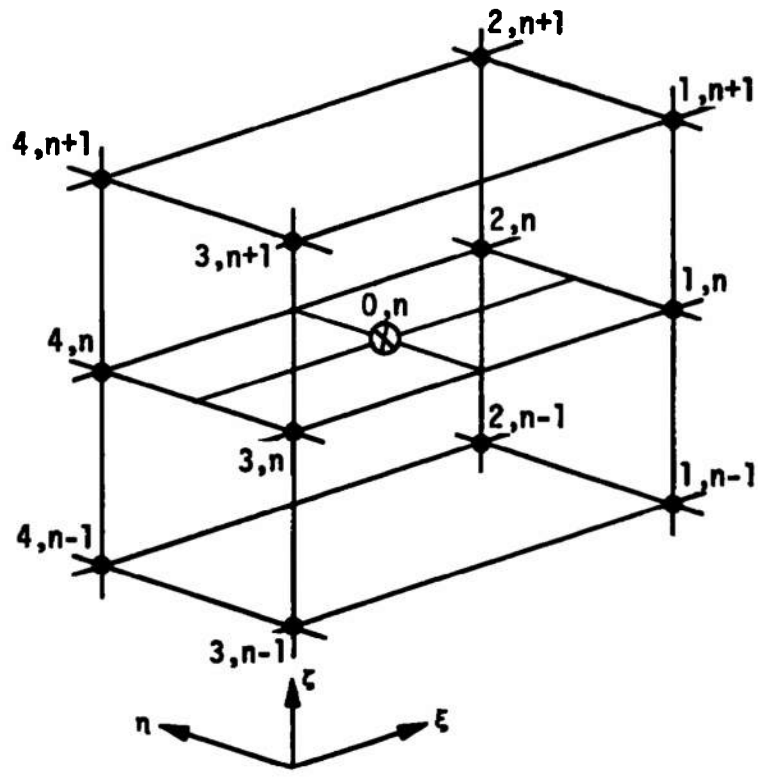

Figure 9. Typical Section of Finite-Difference Grid for $\xi > 0$, $\eta > 0$

are:

$$X_{0,n} = \frac{X_{3,n} + X_{2,n}}{2} + O(\Delta^2)$$

$$\left(\frac{\partial X}{\partial \xi}\right)_{0,n} = \frac{X_{1,n} + X_{2,n} - X_{3,n} - X_{4,n}}{2\Delta\xi} + O(\Delta^2)$$

$$\left(\frac{\partial X}{\partial \eta}\right)_{0,n} = \frac{X_{2,n} + X_{4,n} - X_{1,n} - X_{3,n}}{2\Delta\eta} + O(\Delta^2)$$

$$\left(\frac{\partial X}{\partial \zeta}\right)_{0,n} = \frac{X_{2,n+1} - X_{2,n-1} + X_{3,n+1} - X_{3,n-1}}{4\Delta\zeta} + O(\Delta^2)$$

$$\left(\frac{\partial^2 X}{\partial \zeta^2}\right)_{0,n} = \frac{X_{2,n+1} - 2X_{2,n} + X_{2,n+1} + X_{3,n+1} - 2X_{3,n} + X_{3,n-1}}{2\Delta\zeta^2} + O(\Delta^2) \quad (60)$$

where $\Delta\zeta$ and $\Delta\eta$ are as previously described, and $\Delta\xi$ is the ξ step-size. In Equations (60), $O(\Delta^2)$ implies that the lowest order terms which have been neglected in the development are of the form of a second-order term in $\Delta\xi$, $\Delta\eta$, and $\Delta\zeta$ times some quantity which is independent of the mesh spacing.

The substitution of Equations (60) into Equation (58) yields the standard form of the finite-difference equation as

$$X_{2,n} = A_{X,n}\, X_{2,n+1} + B_{X,n}\, X_{2,n-1} + C_{X,n} \quad (61)$$

The A, B, and C terms are defined as:

$$A_{X,n} = \frac{AN_{X,n}}{DN_{X,n}}$$

$$B_{X,n} = \frac{BN_{X,n}}{DN_{X,n}}$$

$$C_{X,n} = \frac{CN_{X,n}}{DN_{X,n}} \tag{62}$$

where

$$AN_{X,n} = \frac{1}{2\Delta\zeta^2} + \frac{\alpha_{X1}}{4\Delta\zeta}$$

$$BN_{X,n} = \frac{1}{2\Delta\zeta^2} - \frac{\alpha_{X1}}{4\Delta\zeta}$$

$$CN_{X,n} = \frac{1}{2\Delta\zeta^2}\ (X_{3,n+1} - 2X_{3,n} + X_{3,n-1})$$

$$+ \frac{\alpha_{X1}}{4\Delta\zeta}\ (X_{3,n+1} - X_{3,n-1}) + \frac{\alpha_{X2}}{2}\ X_{3,n}$$

$$+ \alpha_{X3} + \frac{\alpha_{X4}}{2\Delta\zeta}\ (X_{1,n} - X_{3,n} - X_{4,n})$$

$$+ \frac{\alpha_{X5}}{2\Delta\eta}\ (X_{4,n} - X_{3,n} - X_{1,n})$$

$$DN_{X,n} = \frac{1}{\Delta\zeta^2} - \frac{\alpha_{X2}}{2} - \frac{\alpha_{X4}}{2\Delta\xi} - \frac{\alpha_{X5}}{2\Delta\eta} \tag{63}$$

The equations represented by Equation (61) are solved for $X_{2,n}$ $(1 < n < NZ)$ by the application of Equations (50). The α terms in Equations (63) are evaluated at the point (0,n) through the use of Equations (60), and are

treated as known quantities through the iteration scheme described in the first section of this chapter.

The surface boundary conditions on Φ, G, and θ are as previously described. The outer-edge conditions are determined through the streamline-swallowing analysis in an iteration scheme separate from that involved in the iterative solution of Equations (61). The details of that treatment are given in the following section; however, the basic approach is that the location of the inviscid separating surface at $\xi = \xi_2$, $\eta = \eta_2$ is initially approximated in some manner. The outer-edge conditions so determined are used in the solution of the boundary-layer equations, and that solution is used to determine again the location of the inviscid separating surface and the concomitant outer-edge conditions. This entire procedure is repeated until a converged value is obtained for the location of the inviscid separating surface. This procedure was mentioned previously with respect to Figure 5, page 29.

In addition to determining u_e, v_e, etc. on the inviscid separating surface, the value of du/dy in the inviscid flowfield at $\xi = \xi_2$, $\eta = \eta_2$ on the inviscid separating surface is obtained for use in the outer-edge boundary condition on Φ as given in Equation (34).

IV. NUMERICAL TREATMENT OF THE STREAMLINE-SWALLOWING PHENOMENON

In Section IV of Chapter II a mass-balance scheme is presented through which the boundary-layer outer-edge conditions may be determined in a manner which considers the entrainment of the inviscid flow by the

boundary layer. The crux of the scheme is in the determination of the height above the body surface of the surface in the inviscid flowfield which separates that part of the inviscid flow which is entrained by the boundary layer from that part of the flow which is not entrained by the boundary layer. The approach of this investigation has been such that no explicit treatment need be given to the streamline-swallowing problem along the two surfaces $\xi = 0$ and $\eta = 0$; however, the phenomenon is treated by satisfying Equation (35) at all points where $\xi > 0$ and $\eta > 0$.

In particular, with reference to Figure 5, page 29, the general treatment is that with solutions to the boundary-layer equations having been determined at points 1, 3, and 4, the height of the inviscid separating surface is determined at $\xi = \xi_2$, $\eta = \eta_2$, through iteration, such that the final solution of the boundary-layer equations obtained at point 2 satisfies Equation (35). The iteration is necessary because the height of the inviscid separating surface is needed in order to obtain the outer-edge conditions required to solve the boundary-layer equations, while at the same time the solution of the boundary-layer equations is needed in order to obtain the location of the inviscid separating surface. With $\xi_3 = \xi_4$ initially at $\xi = 0$, and $\eta_1 = \eta_3$ initially at $\eta = 0$, the scheme may be applied at $\xi = \xi_2$, $\eta = \eta_2$ and marched around the body in the direction of increasing η. The scheme is then applied one step further down the body in the ξ direction, and may be repeated until the desired length of body has been treated.

In applying Equation (35), the integrals given in Equations (36) and (37) are treated by appropriate finite-difference schemes. The

general form of Equations (36) and (37) (and their non-dimensional counterparts, which are used in the actual computations) is

$$\dot{m}_{a-b} = \int_{\lambda_a}^{\lambda_b} \int_{o}^{1} f(\lambda,\zeta)d\zeta \; g(\lambda)d\lambda \tag{64}$$

where λ represents either ξ or η. These integrals are treated as

$$\dot{m}_{a-b} = \left(\frac{j_a + j_b}{2}\right) \int_{\lambda_a}^{\lambda_b} g(\lambda)d\lambda \tag{65}$$

where

$$j_a = \int_{o}^{1} f(\lambda_a,\zeta)d\zeta$$

$$j_b = \int_{o}^{1} f(\lambda_b,\zeta)d\zeta \tag{66}$$

The integral in Equation (65) is in all cases a form which can be evaluated exactly; the integrals in Equations (66) have been evaluated using trapezoidal rule numerical integration. The indicated treatment of the ζ integral in Equation (64) should be adequate since the functions indicated by $f(\lambda,\zeta)$ are slowly varying functions of ξ or η, as the case may be.

In iterating on the height of the inviscid separating surface

at point 2, if a solution of the boundary-layer equations at point 2 is known, generally based on a previous iteration, then all of the terms in Equation (35) can be evaluated, using Equations (64), (65), and (66), except for $\dot{m}^*_{1-2}$ and $\dot{m}^*_{2-4}$. Writing Equation (35) as

$$\dot{m}^*_{1-2} + \dot{m}^*_{2-4} = \dot{m}'_{1-2} + \dot{m}'_{2-4} + \dot{m}^*_{1-3} + \dot{m}^*_{3-4} - \dot{m}'_{1-3} - \dot{m}'_{3-4} \tag{67}$$

the right-hand side can be evaluated directly. The sum $\dot{m}^*_{1-2} + \dot{m}^*_{2-4}$ can then be determined as a function of the distance in the inviscid flowfield above the body surface at point 2. Finally, the distance which yields the equality in Equation (67) can be determined, and this distance is the height of the inviscid separating surface at point 2. From this the outer-edge conditions to be imposed on the boundary-layer equations may be determined and the boundary-layer equations solved again. This procedure is repeated until the desired degree of convergence is attained.

In casting Equations (36) and (37) into their equivalent non-dimensional forms, the boundary-layer mass-flow integrals take on a multiplier of the square root of the freestream Reynolds number based on the arbitrary reference length $\bar{L}$, while the mass-flow integrals for the inviscid flow have the Reynolds number itself as a coefficient. This has the result that the treatment of the problem is not completely independent of the freestream Reynolds number when streamline swallowing is being considered. It is possible in principle, however, to perform calculations for one value of Re and to apply the results obtained to cases which have different freestream Reynolds numbers based on body length. This can be done by choosing for each case an appropriate value

for the reference length $\bar{L}$, and using, in terms of ξ, only a part of the solution which was obtained. However, to apply this procedure generally would mean that the one computation performed would need to consider on the one hand a body of sufficient length (in terms of ξ) and on the other hand still have a sufficiently fine ξ-grid such that the use of only a part of the results for low Re cases would be meaningful (i.e., have reasonable resolution). Rather than use this route, the approach of this investigation has been to let $\bar{L}$ take a fixed value, regardless of Re, and then to perform a different set of computations for each different Reynolds number condition which is considered for a given body.

CHAPTER IV
RESULTS OF CALCULATIONS

In this chapter are presented the results of numerical experiments concerning the behavior of the solution method described in the previous chapter, comparisons of results from the present method with experimental data and the results of other computations, and the results of calculations which demonstrate the effects of streamline swallowing on computed boundary-layer data.

I. NUMERICAL EXPERTIMENTS

A series of calculations were performed to investigate grid spacing, convergence criteria, and other factors involved in applying the finite-difference solution technique described in Chapter III. Generally, these calculations were performed for the case of a 10-degree half-angle cone at an angle of attack of eight degrees in a Mach 7.95 flow. A wall-to-total enthalpy ratio of 0.4 and a value of $Re = 1.26 \times 10^6$ (based on $\bar{L} = 1$ foot) were used in the calculations. This case is one which has been investigated experimentally by Tracy (21).

Practical values for the number of grid points in the ζ and η directions and a convergence criterion for the iterative solution technique were determined by considering the classical similarity solutions obtained at $\xi = 0$. Results obtained with 51 ζ-points from the surface to $\zeta = 1$ agreed to within less than one-half of one percent with solutions

obtained with 101 and 251 points; therefore, 51 ζ-points were used in all calculations. Results obtained using from 21 to 61 η-points from $\eta = 0$ to $\eta = \pi$ agreed to within the same tolerance; therefore, 37 η-points were used, yielding a convenient value of $\Delta\eta = 5$ degrees.

The convergence of the iteration resulting from the linearization involving the α terms (e.g., between Equations (41) and (44)) was determined by testing the change in the solution between successive iterations. It was observed that the surface value of Φ was the most sensitive part of the entire solution, and that when the surface value of Φ had converged the entire solution was also converged. Specifically, the iteration was terminated when the surface value of Φ varied less than 0.01 percent between successive iterations. Results obtained using a convergence tolerance of 0.001 percent varied less than 0.1 percent from those obtained using a tolerance of 0.01 percent.

When the outer-edge conditions imposed on the boundary layer were the classical inviscid surface data, the ξ-step used in marching the solution down the body did not materially affect the results obtained, and the similarity solutions obtained at $\xi = 0$ were repeated at each value of ξ considered. When streamline swallowing was considered, however, this was not the case. The use of a ξ-step which began at $\Delta\xi = 0.05$ and increased relatively rapidly with ξ resulted in small but noticeable oscillations (with respect to ξ) appearing in the solution. The use of a ξ-step having a constant value of 0.05 yielded well-behaved solutions, and this value was used in subsequent calculations.

The convergence of the iteration described in Section IV of

Chapter III for the determination of the height of the inviscid separating surface above the body surface was determined through a comparison of the values of the height of the inviscid separating surface obtained from successive iterations. The iteration was deemed to be sufficiently converged when successive values differed by no more than 0.1 percent.

van Driest (22) employed a Crocco-variables formulation for the treatment of the boundary-layer flow over a flat plate. In this formulation he encountered a singularity in the solution at the outer edge of the boundary layer; however, he was able to cope with the problem through the use of appropriate numerical devices. The origin of the problem lay in the classical outer-edge boundary condition of zero velocity gradient, which is analogous to $\Phi = 0$ at $\zeta = 1.0$ in the present treatment. In van Driest's treatment this quantity appeared in the denominator of a term which was evaluated at the outer edge of the boundary layer, and yielded the singularity. In the present treatment no such situation arises in the solution of the governing equations, although it does arise in the determination of the distance normal to the body surface, through the use of Equation (30). The problem here is equivalent to requiring that the outer edge of the boundary layer be at a distance of infinity from the body surface, a mathematical requirement for an asymptotic approach of the solution to its outer-edge boundary condition. In the present investigation, for cases where $\Phi = 0$ at $\zeta = 1.0$, the denominator in the integral in Equation (30) was treated in the numerical integration by taking the reciprocal of the average of Φ rather than the average of the reciprocals between successive points. This treatment introduced

no approximations back into the solution; its only result was that the computed location of the outer edge of the boundary layer was a finite distance from the surface. For cases in which streamline swallowing was considered, the entire problem ceased to exist because the value of Φ at $\zeta = 1$ was no longer zero, but some value determined as a part of the overall solution.

For some cases encountered in developing the digital computer program used in this investigation, the direct application of the method of solution described in Chapter III failed to yield a converged solution at $\xi = 0$, $\eta = 0$. Instead, the iteration scheme resulted in an essentially stable oscillation between two different "solutions". This problem was remedied by using a weighted average of the two previous iterations of Φ in evaluating Equations (42), rather than the value obtained from just the preceding iteration. This modification yielded convergence and was used in all subsequent calculations.

A value of one foot has been used for the reference length $\bar{L}$ in all calculations made in this investigation. The fluid under consideration was air, and the values used for the Prandtl number and the ratio of specific heats were 0.7 and 1.4, respectively.

II. COMPARISONS WITH OTHER DATA

In this section results obtained using the present method are compared with results obtained using the method of McGowan and Davis (5) and with experimental data of Tracy (21). The case under consideration is the same as that in the previous section, namely a 10-degree half-angle

cone at 8-degree angle of attack in a Mach 7.95 flow. For this case, the effects of streamline swallowing on the results which are presented were determined to be negligible. This was because of the relatively weak shock associated with the slender body under consideration. For this reason, the computed results presented in this section are from calculations which used the inviscid surface data for the boundary-layer outer-edge conditions.

Figure 10 shows a comparison of the results from the present method with results obtained using the method of McGowan and Davis (5). The similarity forms of the coefficients of longitudinal and lateral skin friction and the Stanton number are presented as functions of the lateral coordinate η. The only noticeable differences between the two sets of results are in the region of the lee side of the body (η > 100 degrees). These differences are attributed to a smoothing scheme used in the method of McGowan and Davis (5) to eliminate certain difficulties encountered in their treatment of the inviscid data which provided the outer-edge boundary conditions for the boundary-layer equations. In spite of this, the agreement between the two sets of results is reasonable.

Figure 11 shows a comparison between the surface pressure distribution around the body as measured by Tracy (21) and that computed using the method of Jones (12). There is excellent qualitative agreement between the two distributions; however, the experimental distribution is greater than the computed one by an almost constant amount. No likely source of a consistent error has been found to explain this difference.

Figure 12 shows a comparison between the measured surface heat-

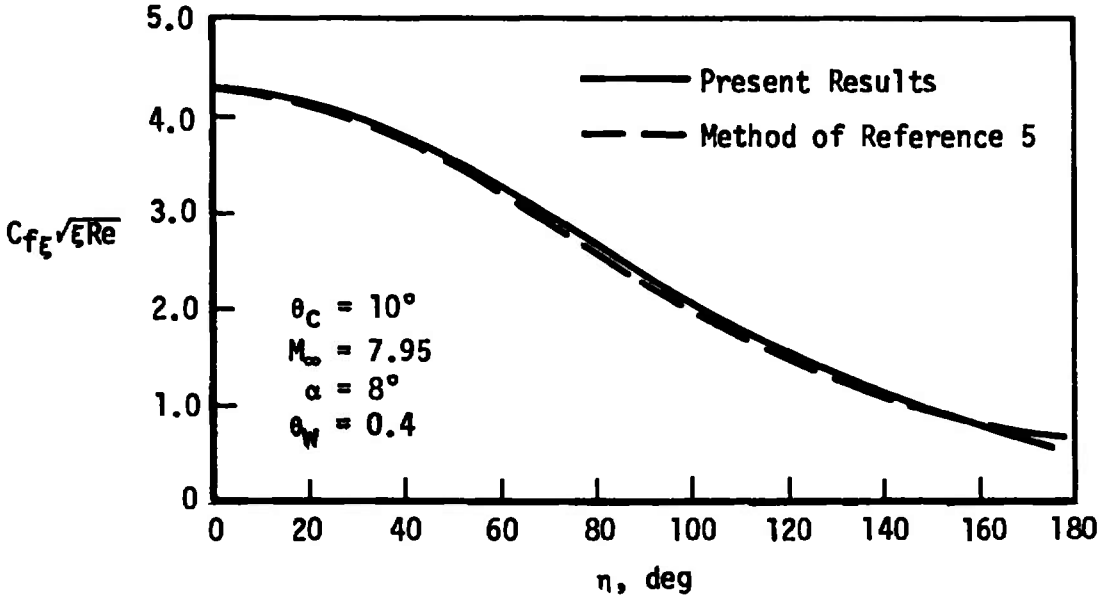

(a) Coefficient of Longitudinal Skin Friction

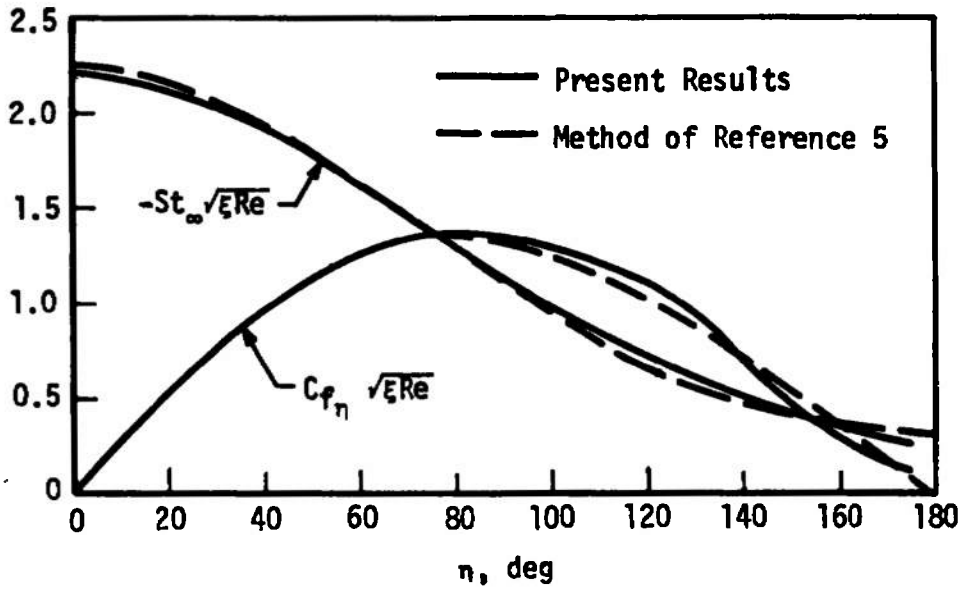

(b) Coefficient of Lateral Skin Friction and Stanton Number

Figure 10. Comparison of Results of the Present Method with Results of the Method of Reference 5

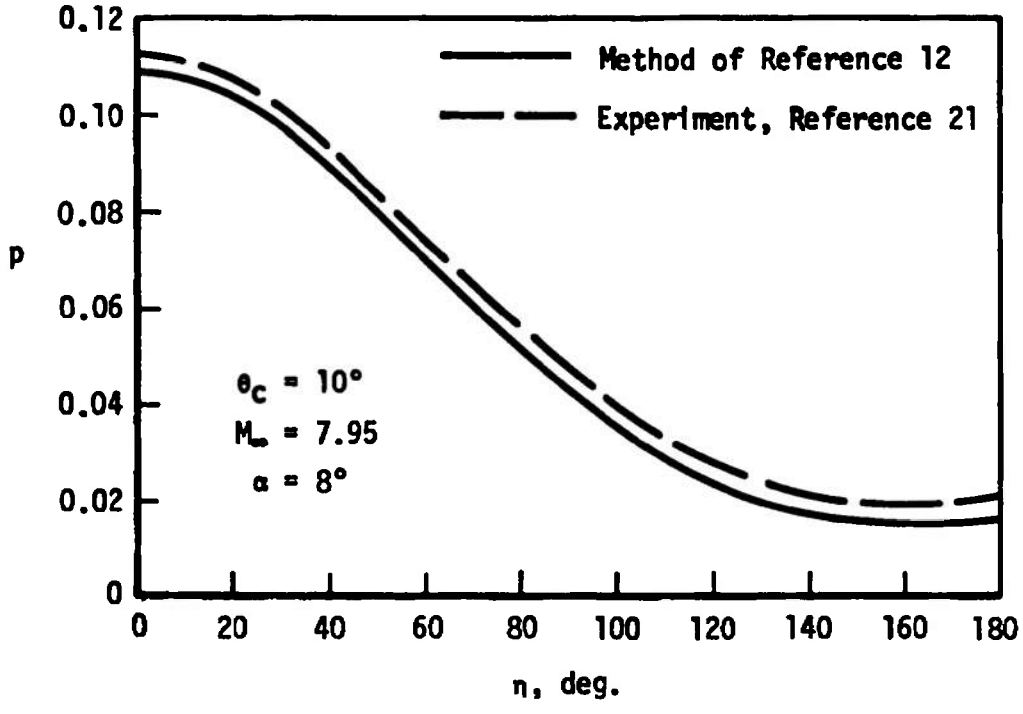

Figure 11. Comparison of Calculated Surface Pressure Distribution with Experimental Data

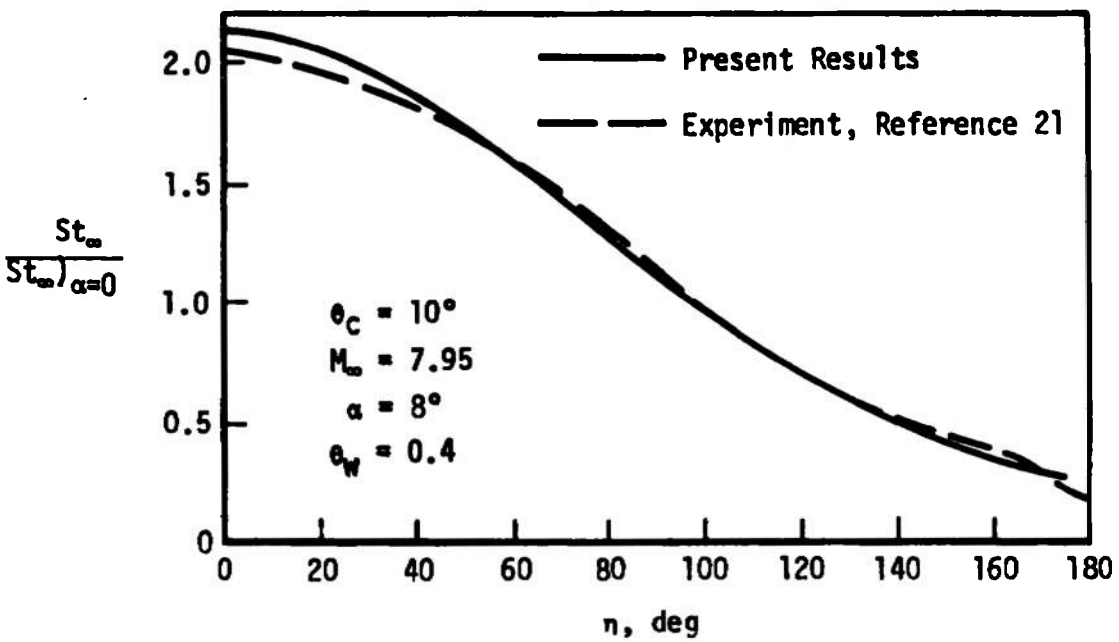

Figure 12. Comparison of Computed Heat-Transfer Distribution with Experimental Data

transfer distribution around the body as reported by Tracy (21) and the heat-transfer distribution computed by the present method. The heat-transfer parameter shown is the Stanton number at angle of attack divided by the Stanton number at zero angle of attack, at the same value of ξ. The measured and computed data shown in Figure 12 agree quite well.

III. EFFECTS OF STREAMLINE SWALLOWING

In this section are presented inviscid flowfield data which indicate conditions for which the influence of streamline swallowing might be significant, the results of computations which demonstrate the effects of streamline swallowing on computed boundary-layer data, and data indicating the relationship between the boundary layer and the corresponding inviscid flowfield.

It was noted in the previous section that, for the case of the 10-degree half-angle cone at 8-degree angle of attack in a Mach 7.95 flow, streamline-swallowing effects on surface heat transfer and skin friction were negligible. This result is indicated by the distributions across the calculated inviscid flowfield of the longitudinal and lateral components of velocity shown in Figure 13. Noting the expanded abscissa scale, it can be seen that, although there is a definite entropy layer near the body surface, the change of the velocity components across this region of large gradients is relatively small. Since the effects of streamline swallowing on computed boundary-layer data are caused by changes of the inviscid data across the entropy layer, small effects of streamline swallowing should be expected for this case, as was found in corresponding

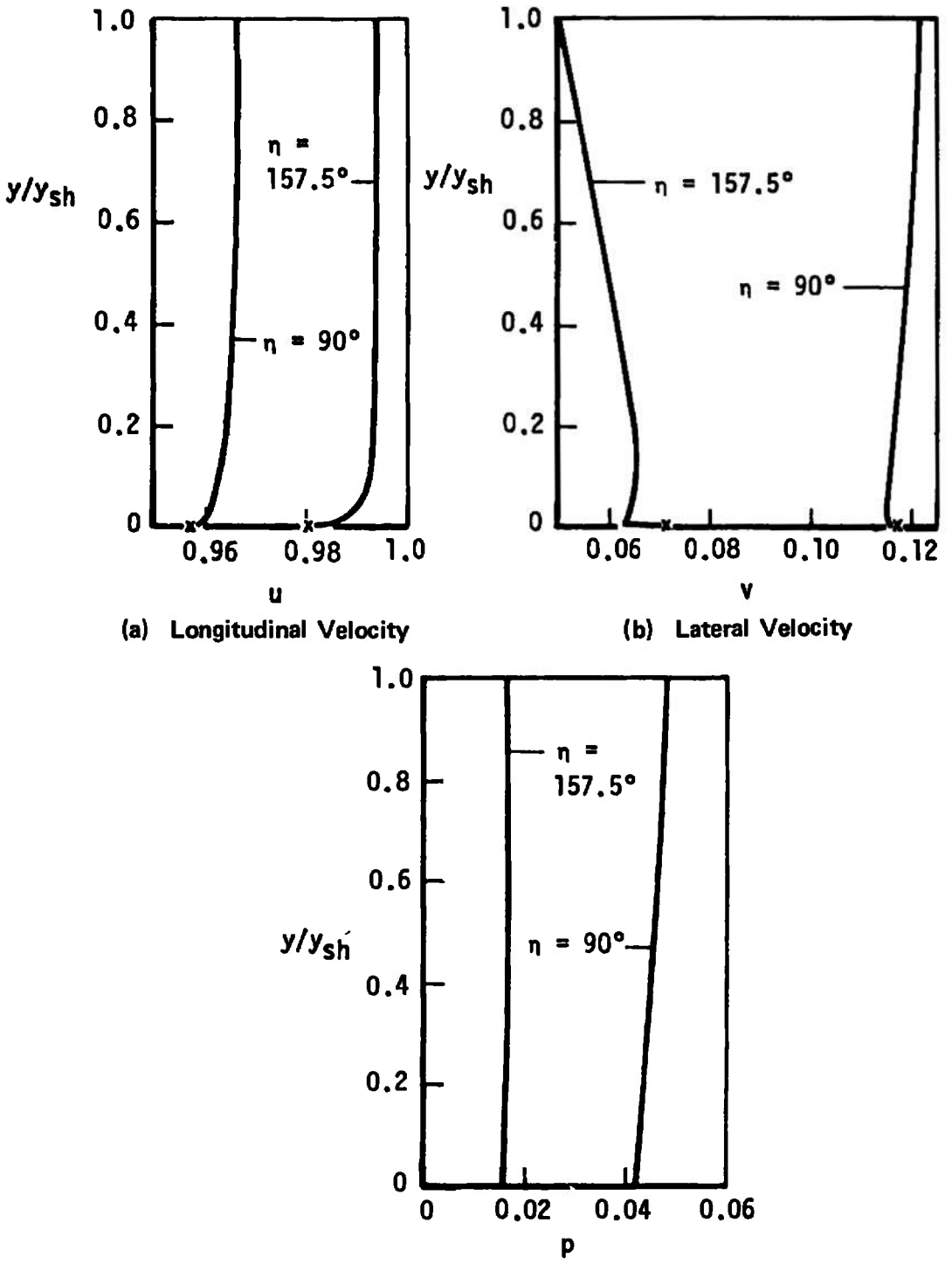

Figure 13. Inviscid Flowfield Data for 10-Degree Cone at 8-Degree Angle of Attack in a Mach 7.95 Flow

calculations. The data at η = 90 degrees and η = 157.5 degrees show the development of the entropy layer as the flow approaches the leeward symmetry plane.

Figure 13 also shows the pressure distribution across the inviscid flowfield. These data and similar data in the succeeding two figures show the relatively small pressure variation across the inviscid flowfield between the body surface and the shock wave

The reason for the small changes of the inviscid flowfield data across the entropy layer for the case shown in Figure 13 is that the slender body is not highly inclined to the freestream flow, and has everywhere a relatively weak bow shock wave. This leads to the difference in the influence of the bow shock on the inviscid flow being relatively small between its strongest and weakest portions, in spite of the high Mach number.

Figure 14 shows computed inviscid flowfield data for a 25-degree half-angle cone at 12.5-degree angle of attack in a Mach 2.0 freestream For this case the low Mach number causes the changes across the entropy layer to be small in spite of the variation in the shock wave inclination being greater than in the previous case.

Figure 15 shows computed inviscid flowfield data for the case of a 25-degree half-angle cone at 12.5-degree angle of attack in a Mach 7.95 freestream. For this condition the variation across the entropy layer of the velocity components is much greater than in either of the two preceding cases, and, therefore, this case has been chosen to demonstrate the effects of streamline swallowing on computed boundary-layer data. The variations

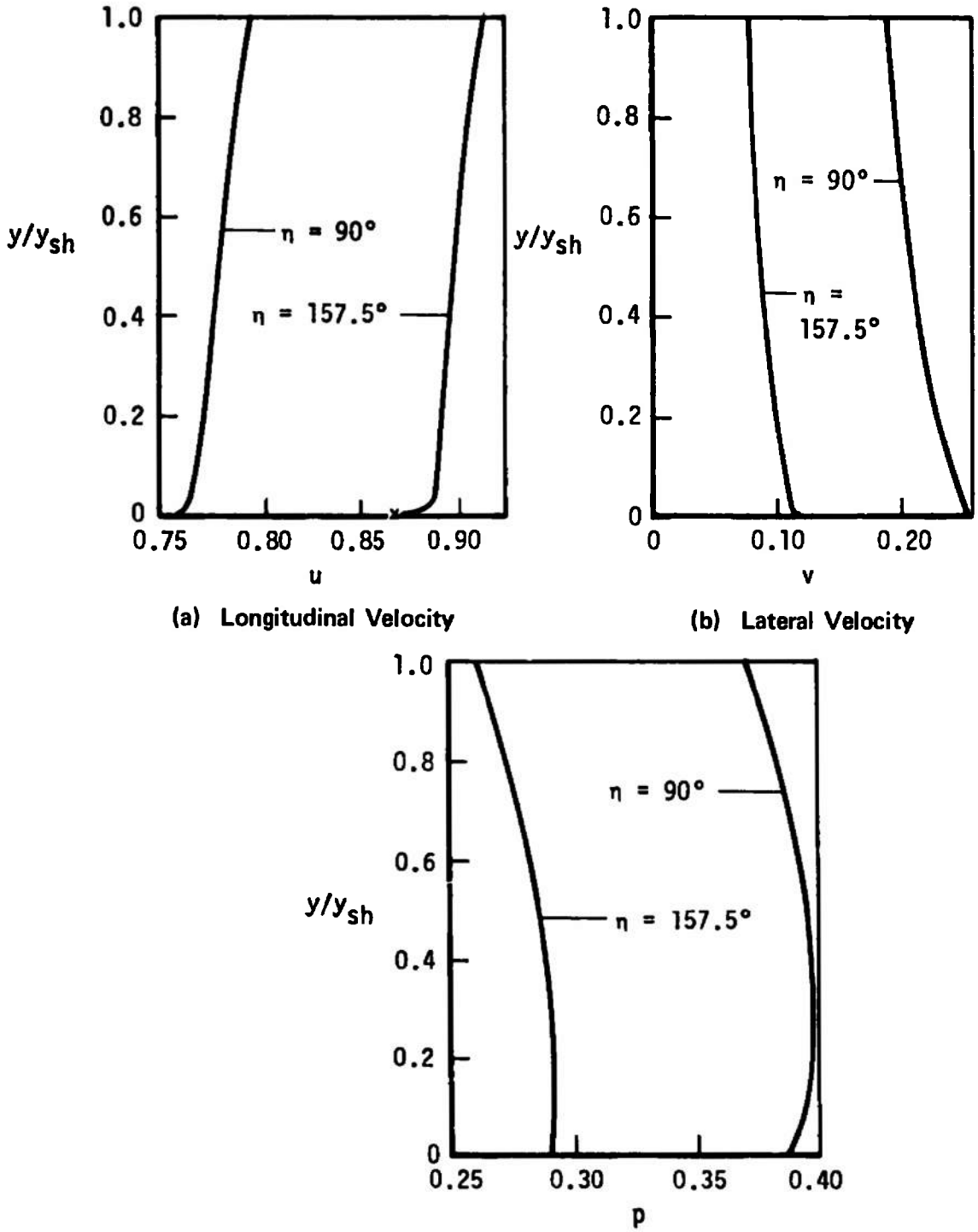

Figure 14. Inviscid Flowfield Data for 25-Degree Cone at 12.5-Degree Angle of Attack in a Mach 2.0 Flow

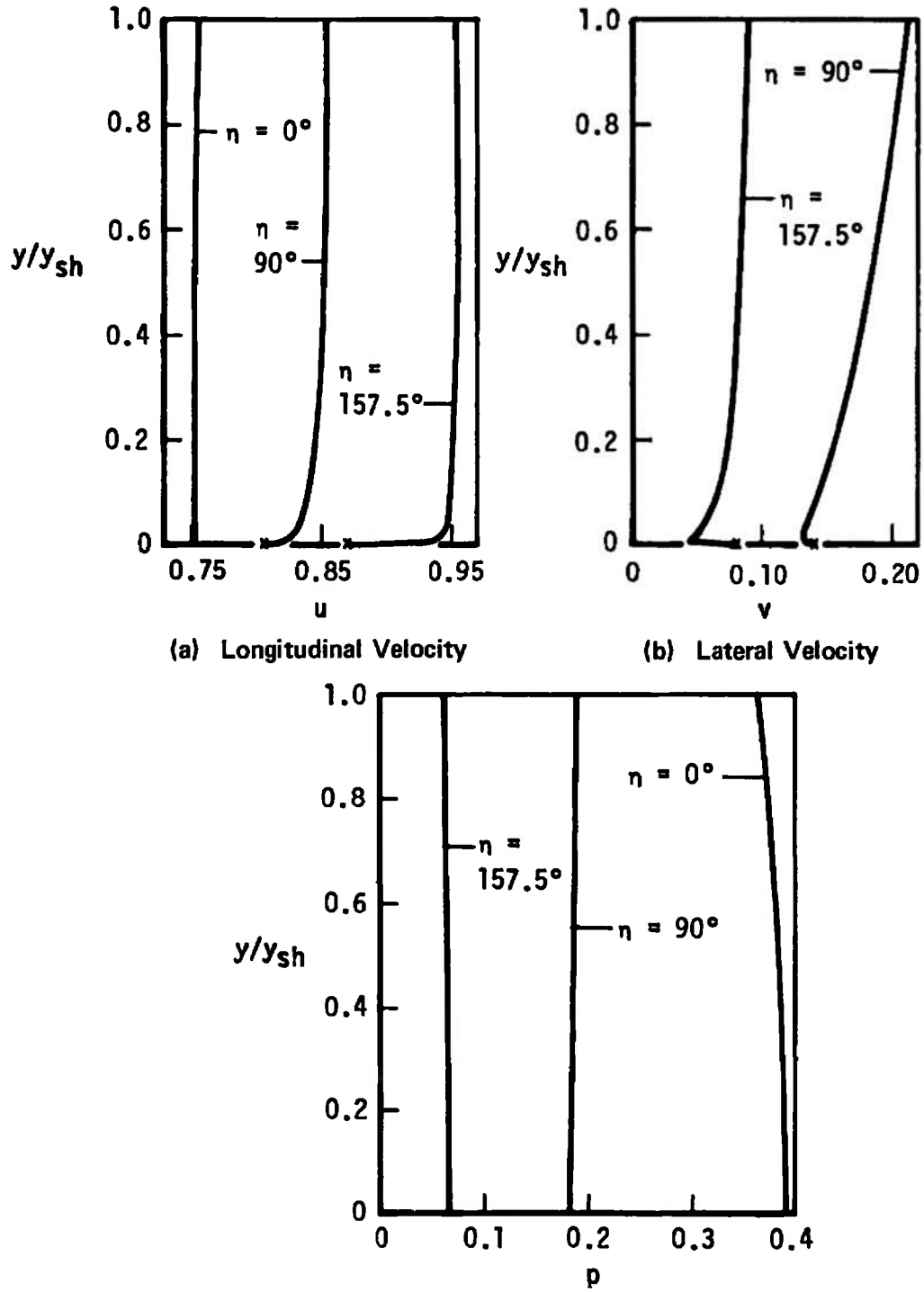

Figure 15. Inviscid Flowfield Data for 25-Degree Cone at 12.5-Degree Angle of Attack in a Mach 7.95 Flow

of the longitudinal velocity component and the pressure across the inviscid flowfield at $\eta = 0$ has been shown in Figure 15 to indicate the uniformity of the inviscid flow there.

For the case of a 25-degree half-angle cone at 12.5-degree angle of attack in a Mach 7.95 flow, calculations have been performed which included the effects of swallowing by the boundary layer of the inviscid flow. A constant value of 0.4 was used for the wall-to-total enthalpy ratio.

Figure 16 shows the variation with η of the coefficients of longitudinal and lateral skin friction and the Stanton number at a value of $\xi = 1.0$. Results are shown from calculations which used the classical isentropic-surface inviscid data for outer-edge boundary conditions and from computations which considered the swallowing by the boundary layer of the inviscid flow. The streamline-swallowing data are for a value of $Re = 1.26 \times 10^4$. The differences between the results with and without streamline swallowing are zero at $\eta = 0$, and increase with increasing η, although the coefficient of lateral skin friction goes to zero at $\eta = 180$ degrees for both cases. The coefficient of longitudinal skin friction is greater at all values of η for the case which includes streamline swallowing, with the difference being on the order of 15 percent on the leeside of the body. The relative values of the two sets of data for the coefficient of lateral skin friction and Stanton number are not uniform with respect to even which is the greater, although the relative difference between the classical results and the streamline-swallowing results attains a maximum of about eight percent for both parameters.

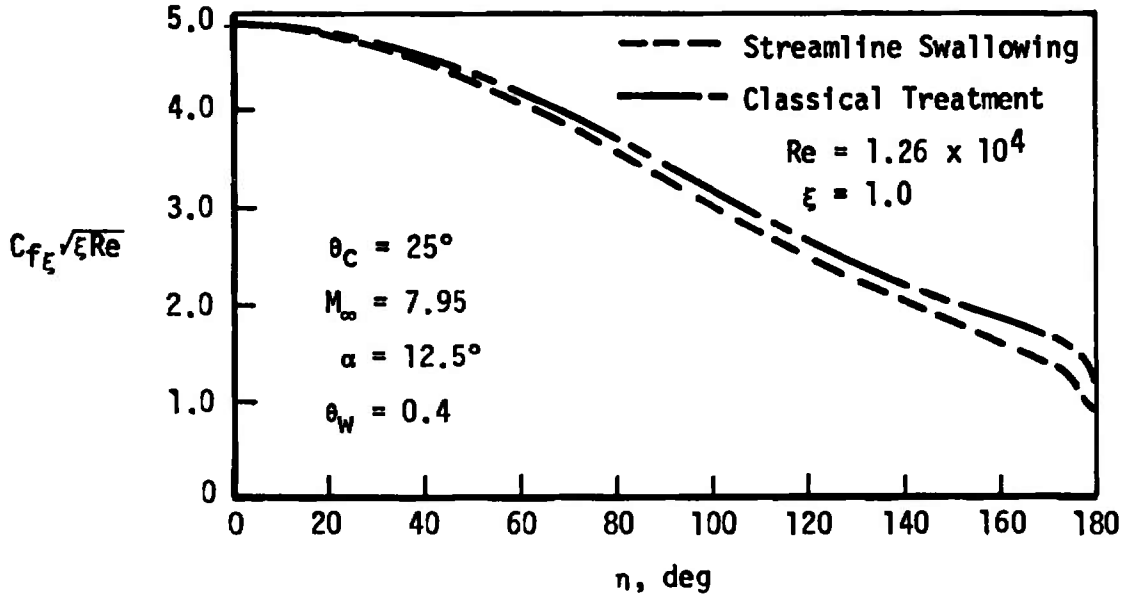

(a) Coefficient of Longitudinal Skin Friction

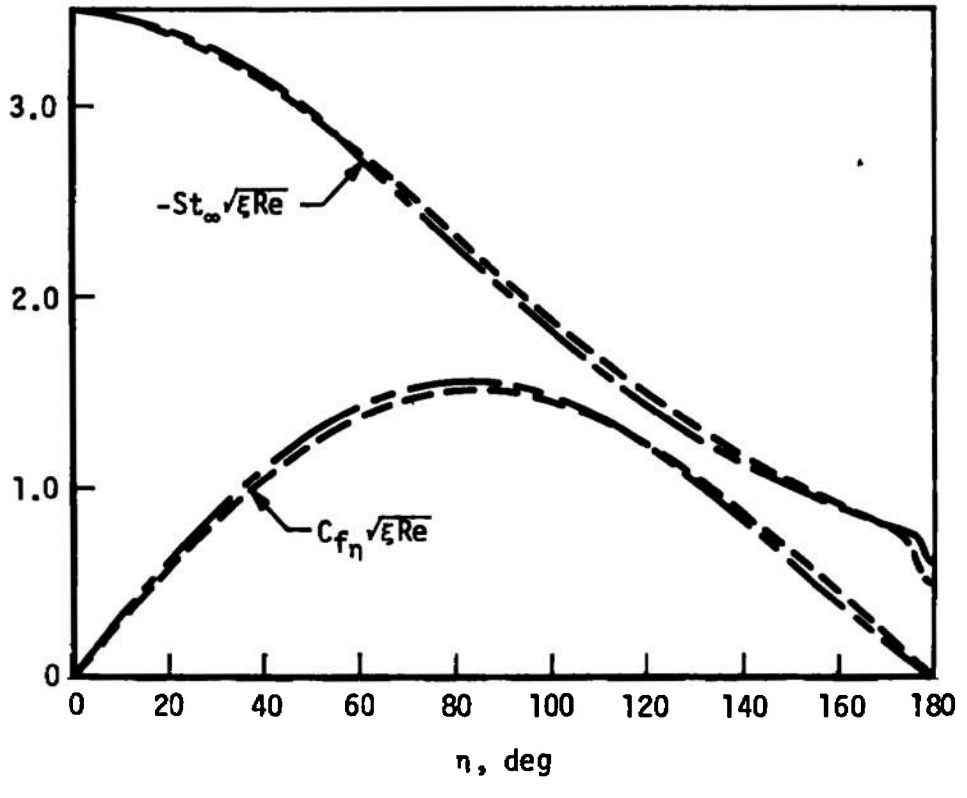

(b) Coefficient of Lateral Skin Friction and Stanton Number

Figure 16. Effects of Streamline Swallowing on Computed Surface Data at a Fixed Value of ξ

Figure 17 shows the longitudinal variation of the coefficients of skin friction and the Stanton number at η = 150 degrees for two values of Re. For Re = 1.26 x 10^6 the coefficient of longitudinal skin friction approaches the classical similarity solution value as ξ increases, while for Re = 1.26 x 10^4 the results are further displaced from the classical results, and do not vary greatly over the length of body considered. Since the boundary-layer growth goes approximately (exactly for similarity solutions) like the square root of ξ, while the inviscid flowfield growth is directly proportional to ξ, in the limit as ξ becomes very large the boundary-layer data based on the streamline-swallowing analysis should approach the results obtained using the classical treatment of the boundary-layer outer-edge conditions. This process is also hastened by increasing Re, and the longitudinal skin-friction data for Re = 1.26 x 10^6 may well be a demonstration of the limiting process.

The lateral skin-friction results, although influenced by the value of Re, do not exhibit the above mentioned approach to the classical treatment result as a limiting case.

Concerning the scaling of the results with respect to ξ and Re (discussed in Section IV of Chapter III), the data for Re = 1.26 x 10^4 on the range $0 \leq \xi \leq 1.0$ should also be the appropriate results for Re = 1.26 x 10^6 on the range $0 \leq \xi \leq 0.01$. In fact, the results so scaled are probably more appropriate than the data shown for Re = 1.26 x 10^6, since for both values of Re the solutions obtained for ξ less than about 0.05 should be considered "starting solutions" rather than accurate results (see Section I of Chapter III).

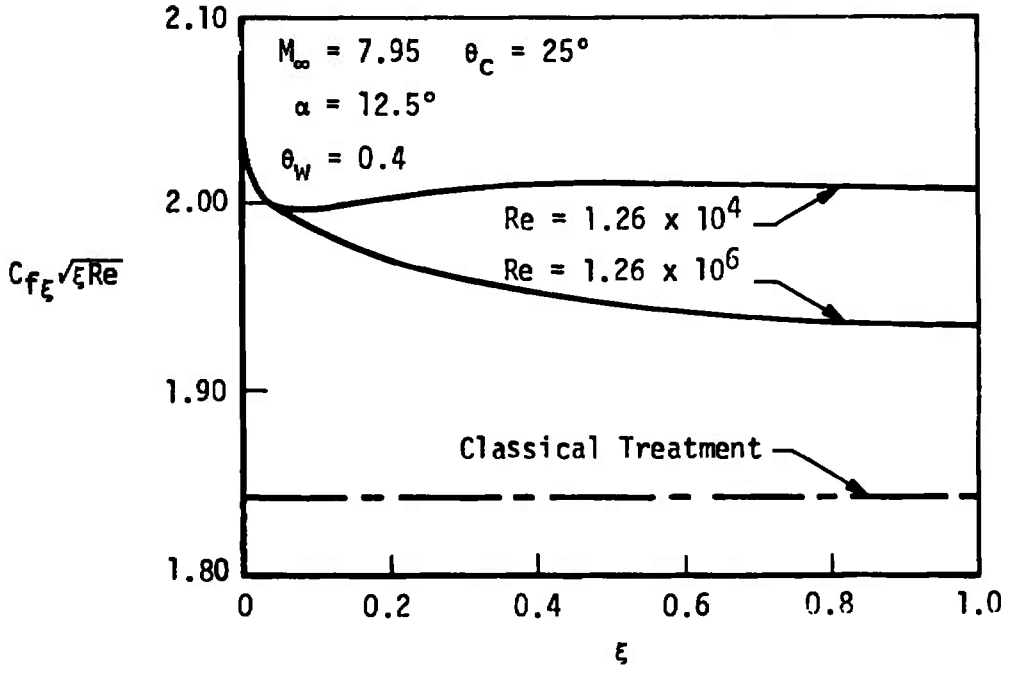

(a) Coefficient of Longitudinal Skin Friction

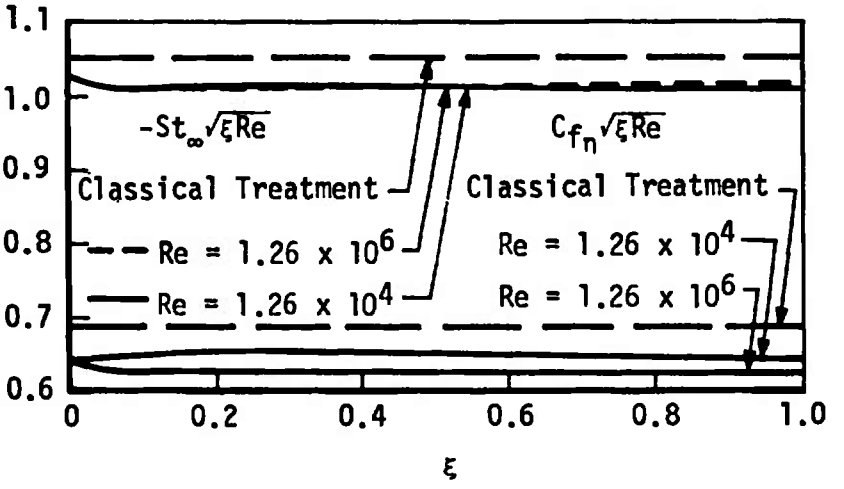

(b) Coefficient of Lateral Skin Friction and Stanton Number

Figure 17. Effects of Streamline Swallowing on Computed Surface Data at η = 150° for Two values of Re

The Stanton number data in Figure 17 exhibit little dependence upon Re, although the results for Re = 1.26×10^6 appear to be tending toward the classical results toward the end of the body considered.

The reason for the small variation with ξ of the results shown in Figure 17, especially for Re = 1.26×10^4, is that the boundary layer has completely swallowed the entropy layer, and the resulting outer-edge boundary conditions being applied to the boundary-layer equations vary only slightly with ξ.

Figure 18 shows boundary-layer profile data at ξ = 1.0 and η = 150 degrees. Shown are the results of computations which include streamline swallowing for Re = 1.26×10^4 and Re = 1.26×10^6 and results obtained using the classical treatment of the outer-edge boundary conditions. The longitudinal velocity profile data approach the classical results as Re increases from 1.26×10^4 to 1.26×10^6. This result follows from y_{ss}/y_{sh} being less for the higher value of Re and from the value of u in the inviscid flowfield varying monotonically between the surface and the shock, as shown in Figure 15, page 77.

The relationship of the lateral velocity profiles for the two values of Re, with respect to the classical result, is different from that of the longitudinal velocity. In fact, because of the behavior of the value of v in the inviscid flowfield (as shown in Figure 15, page 77), the relationship of the results based on the streamline-swallowing treatment to the classical results cannot be predicted beforehand.

The variation of the temperature across the boundary layer shows that when streamline swallowing is included in the analysis the temperature

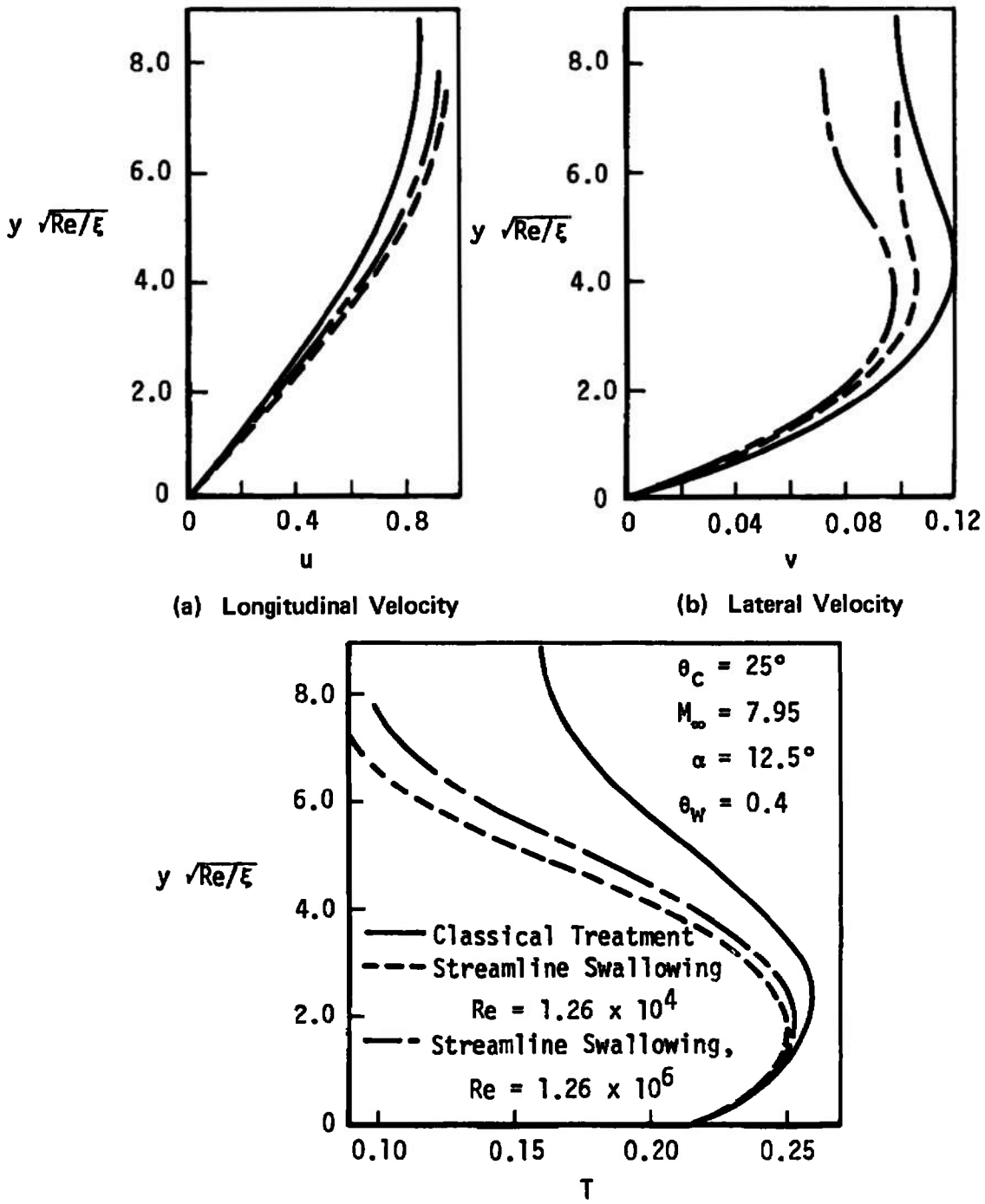

(a) Longitudinal Velocity

(b) Lateral Velocity

(c) Temperature

Figure 18. Boundary-Layer Profile Data at ξ = 1.0, and η = 150°

in the outer part of the boundary layer may be only one-half of the value determined by the classical treatment. Following this, a factor of two applies to the density in the outer part of the boundary layer computed by the two treatments, since, under the assumption of constant pressure with respect to the direction normal to the wall, the density is inversely proportional to the temperature.

Figure 19 shows the variation with η at ξ = 1.0 of the location of the surface in the inviscid flowfield which separates that part of the flow entrained by the boundary layer from that part not entrained by the boundary layer. Results are shown for two values of Re, and the two sets of data differ by approximately a factor of ten, the square root of the ratio of the two Reynolds numbers. If the boundary conditions determined from the inviscid flowfield using the data of Figure 19 did not vary with the distance from the surface, the two sets of data would differ by a factor of exactly ten at each value of η.

Figure 20 shows the variation with ξ at η = 150 degrees of the location of the inviscid separating surface for the same two conditions considered in Figure 19. In addition to the previously mentioned ratio of approximately ten between the data for the two values of Re, these results also show that y_{ss}/y_{sh} varies approximately as the inverse of the square root of ξ. This follows from the boundary layer's growth being proportional to the square root of ξ while the inviscid flowfield grows in direct proportion to ξ. Comparison of Figures 20 and 15, page 77, shows that for both values of Re the boundary layer has completely swallowed the inviscid entropy layer. In fact, these results indicate that a value of Re x ξ in

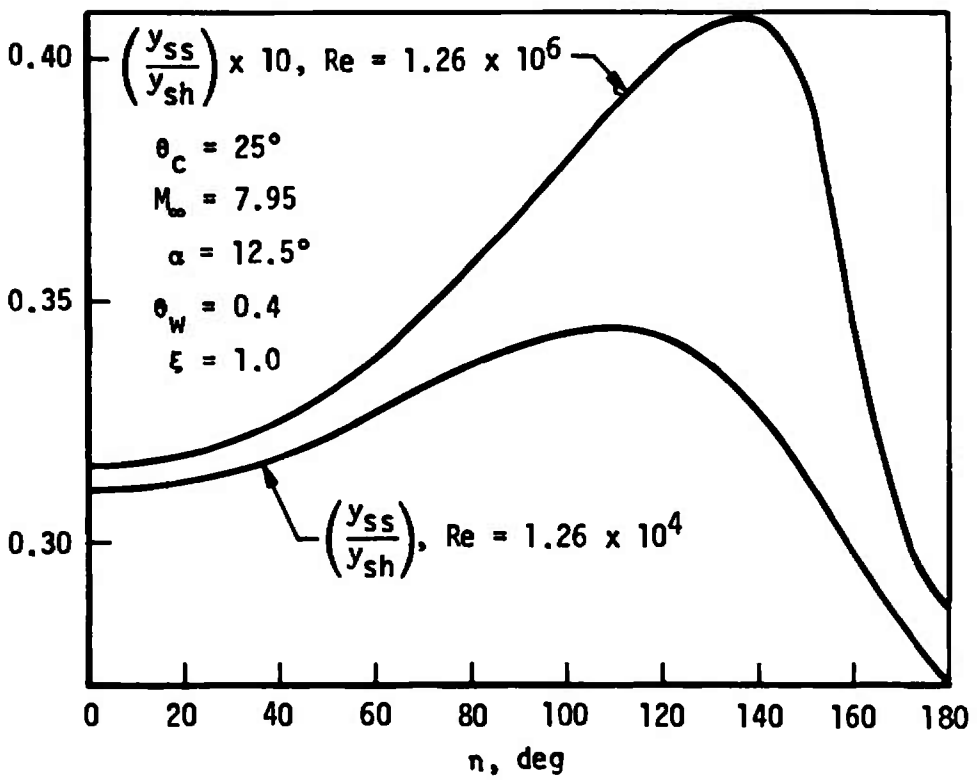

Figure 19. Location of the Inviscid Separating Surface for Two Values of Re at a Fixed Value of ξ

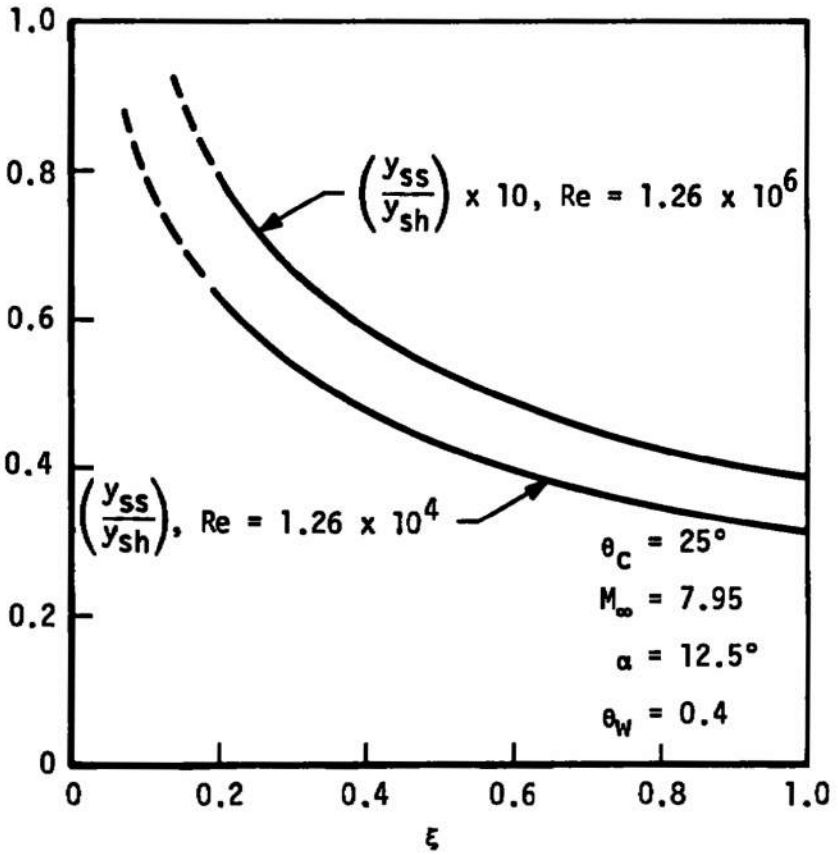

Figure 20. Location of the Inviscid Separating Surface for η = 150° and Two Values of Re

excess of 1×10^9 would have to be attained before the resulting boundary conditions determined for the boundary-layer equations would reach their classical inviscid surface values.

Although the displacement effect of the boundary layer on the inviscid flow has not been considered in this investigation, the displacement thickness over the body is easily found from the results of the streamline-swallowing analysis. Considering the displacement thickness as the mass-flow defect thickness between the inviscid flow and the boundary-layer flow over a body, in the terminology of this investigation the nondimensional displacement thickness, $\delta^* = \bar{\delta}^*/\bar{L}$, is the value of y in the boundary layer at $\zeta = 1$ minus the value of y on the inviscid separating surface at the same value of ξ and η.

The displacement thickness determined in this manner is shown in Figure 21 for $\xi = 1.0$ and two values of Re. The radial coordinate in Figure 21 is the distance normal to the body surface, not the conventional cylindrical radial coordinate; however, this figure does properly illustrate the relative locations of the shock wave, the body surface, and the displacement thickness for the two values of Re considered. For Re = 1.26×10^6 the displacement thickness is small around the entire body, and displacement effects on the inviscid flow should be negligible. For Re = 1.26×10^4, however, the displacement thickness does become significant on the lee side of the body, and displacement effects on the inviscid flow are probably not negligible for this condition.

Figure 22 shows the displacement thickness variation with ξ at η = 150 degrees for two values of Re. These data show that the displacement

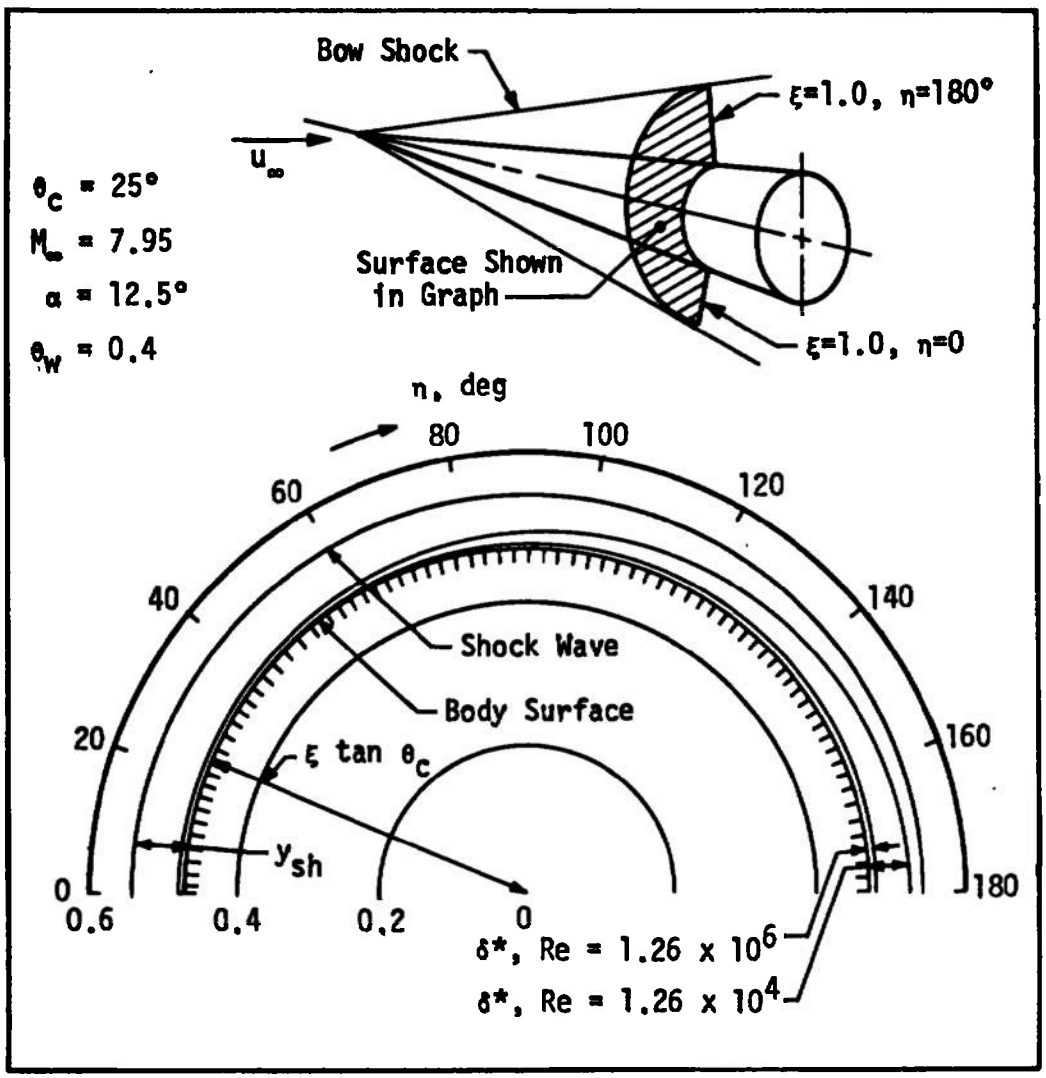

Figure 21. Displacement Thickness Distribution at ξ = 1.0 for Two Values of Re

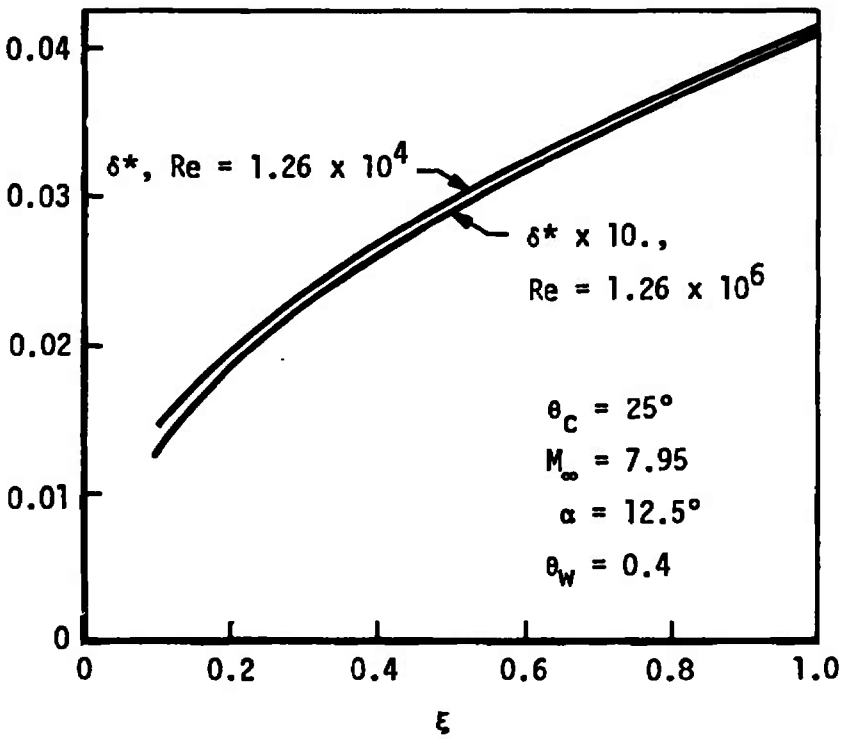

Figure 22. Displacement Thickness Distribution at η = 1.50° for Two Values of Re

thickness is approximately proportional to the inverse of the square root of Re and to the square root of ξ. For the classical similarity solution treatment of the problem the displacement thickness is proportional to the square root of the ratio of ξ to Re, and this rule is approximately valid for the data in Figure 21, page 88, also.

The results presented in this chapter have shown that the influences of streamline swallowing on computed boundary-layer data for cones at angle of attack are not insignificant, and should be considered when accurate flowfield calculations are desired.

Some authors (e.g., Rainbird (23)) have noted that the inviscid surface data are not generally appropriate for use as the outer-edge boundary conditions for the boundary-layer equations in cases such as considered herein, and they have suggested that data from the inviscid flowfield at some (arbitrary) location outside the entropy layer be used. In fact, however, this would indeed be an arbitrary and inexact procedure when compared with the matching procedure used herein to determine the location in the inviscid flowfield at which the boundary-layer outer-edge boundary conditions should be taken.

CHAPTER V
CONCLUSIONS

The three-dimensional compressible laminar boundary-layer equations have been transformed into a general Crocco-variables form, and these equations were particularized to the case of a right circular cone at angle of attack. A method was presented for determining the outer-edge boundary conditions to be applied to the boundary-layer equations through a mass-flow balance between the boundary layer and the inviscid flow over the body.

A finite-difference technique was formulated for solving the resulting set of governing equations and treating the streamline-swallowing phenomenon. The second-order accurate set of coupled nonlinear difference equations were solved in an iteration scheme which employed an efficient algorithm especially suited to their form.

The general treatment of the problem and the method of solution were verified by the good agreement obtained between results from the present method and both experimental data and results from another method of computation. These comparisons were performed for conditions under which the effects of streamline swallowing were insignificant. Unfortunately, no experimental data have been found for conditions which demonstrate the effects of streamline swallowing on measured quantities.

Results were presented which showed that for sufficiently high Mach number and bow shock strength variation, streamline swallowing has a

significant influence on computed boundary-layer data. Streamline swallowing should, therefore, be included in three-dimensional boundary-layer analyses for supersonic and hypersonic conditions when accurate results are desired, even for conical bodies. The treatment of boundary-layer separation and transition from laminar to turbulent flow in a three-dimensional boundary layer are two obvious instances where streamline swallowing should significantly influence boundary-layer computations.

A number of extensions of this investigation present themselves; among them are:

1. Consideration of surface mass-transfer effects, particularly as a simulation of ablation.
2. Consideration of streamline swallowing on blunt-nosed bodies at angle of attack.
3. Treatment of turbulent boundary layers, as appropriate models for the turbulent boundary layer are developed.

One final recommendation is that an investigation be undertaken of the feasibility of treating, in the three-dimensional case, the entire region between the body and the shock wave by a single set of equations which would be valid for both the viscous and inviscid regions, as has been done by Davis (24) for an axisymmetric flow situation. Such a treatment would automatically consider both the streamling-swallowing effect and the displacement effect which should be included in analyses for low Reynolds number cases.

BIBLIOGRAPHY

1. Cooke, J. C., and M. G. Hall. "Boundary Layers in Three Dimensions," Progress in Aeronautical Science, A. Ferri, D. Kuchemann, and L. H. G. Sterne, editors. Vol. 2. Oxford: Pergamon Press, 1962. Pp. 221-282.

2. Stewartson, K. The Theory of Laminar Boundary Layers in Compressible Flow. Oxford: Oxford University Press, 1964.

3. Libby, P. A. "Three-Dimensional Boundary Layer with Uniform Mass Transfer," The Physics of Fluids, 12:408-417, February, 1969.

4. Reshotko, E., and I. E. Beckwith. "Compressible Laminar Boundary Layer Over a Yawed Infinite Cylinder with Heat Transfer and Arbitrary Prandtl Number," National Advisory Committee for Aeronautics Report 1379, Lewis Flight Propulsion Laboratory, Cleveland, Ohio, 1958.

5. McGowan, J. J., III, and R. T. Davis. "Development of a Numerical Method to Solve the Three-Dimensional Compressible Laminar Boundary-Layer Equations with Application to Elliptical Cones at Angle of Attack," Aerospace Research Laboratories ARL 70-0341, Wright-Patterson Air Force Base, Ohio, December, 1970.

6. Moore, F. G., and F. R. DeJarnette. "Viscous Flow-Field Calculations on Pointed Bodies at Angle of Attack in Nonuniform Freestreams." American Institute of Aeronautics and Astronautics Paper No. 71-624, AIAA Fourth Fluid and Plasma Dynamics Conference, Palo Alto, California, June, 1971.

7. Ferri, A. "Some Heat Transfer Problems in Hypersonic Flow," Aeronautics and Astronautics, N. J. Hoff and W. G. Vincenti, editors. New York: Pergamon Press, 1960. Pp. 344-377.

8. Mayne, A. W., Jr., and J. C. Adams, Jr. "Streamline Swallowing by Laminar Boundary Layers in Hypersonic Flow," Arnold Engineering Development Center TR-71-32, Arnold Air Force Station, Tennessee, March, 1971.

9. Fannelop, T. K., and G. D. Waldman. "Displacement Interaction and Flow Separation on Cones at Incidence to a Hypersonic Stream." Paper No. 21 presented at the Advisory Group for Aerospace Research & Development Specialists' Meeting on "Hypersonic Boundary Layers and Flow Fields," London, England, May, 1968.

10. DaForno, G. "Sharp Cones at Hypersonic Speed and Small Angle of Attack," General Applied Sciences Laboratories TM-164, Westbury, Long Island, New York, September, 1967.

11. Raetz, G. S. "A Method of Calculating Three-Dimensional Laminar Boundary Layers of Steady Compressible Flows," Northrop Aircraft Report NAI-58-73, Hawthorne, California, December, 1957.

12. Jones, D. J. "Numerical Solutions of the Flow Field for Conical Bodies in a Supersonic Stream," National Research Council of Canada Aeronautical Report LR-507, Ottawa, Canada, July, 1968.

13. Mager, A. "Three-Dimensional Laminar Boundary Layers," Theory of Laminar Flows, High Speed Aerodynamics and Jet Propulsion, Vol. IV, F. K. Moore, editor. Princeton, New Jersey: Princeton University Press, 1964. Pp. 286-438.

14. Crocco, L. "Lo Strato Limite Laminare nei Gas," Monographic Scientifiche di Aeronautica, No. 3, October, 1946.

15. Der, J., Jr., and G. S. Raetz. "Solution of General Three-Dimensional Laminar Boundary-Layer Problems by an Exact Numerical Method." Institute of the Aerospace Sciences Paper No. 62-70, presented at IAS Thirtieth Annual Meeting, New York, January, 1962.

16. Wang, K. C. "On the Determination of the Zones of Influence and Dependence for Three-Dimensional Boundary-Layer Equations," Journal of Fluid Mechanics, 48:397-404, 1971.

17. Crank, J., and P. Nicholson. "A Practical Method for Numerical Evaluation of Solutions of Partial Differential Equations of the Heat-Conduction Type," Proceedings of the Cambridge Philosophical Society, 43:50-67, 1947.

18. Dwyer, H. A. "The Analysis and Calculation of the Three-Dimensional Boundary Layer Over a Sharp Cone at Angle of Attack." Report prepared under Sandia Corporation Contract No. 48-7084 by the Department of Mechanical Engineering, University of California, Davis, California, 1969.

19. Patankar, S. V., and D. B. Spalding. "A Finite-Difference Procedure for Solving the Equations of the Two-Dimensional Boundary Layer," International Journal of Heat and Mass Transfer, 10:1389-1411, October, 1967.

20. Krause, E. "Comment on 'Solution of a Three-Dimensional Boundary-Layer Flow with Separation'," AIAA Journal, 7:575-576, March, 1969.

21. Tracy, P. P. "Hypersonic Flow Over a Yawed Circular Cone," California Institute of Technology Graduate Aeronautical Laboratories Memorandum No. 69, Pasadena, California, August, 1963.

22. van Driest, E. R. "Convective Heat Transfer in Gases," Turbulent Flows and Heat Transfer, High Speed Aerodynamics and Jet Propulsion, Vol. V, C. C. Lin, editor. Princeton, New Jersey: Princeton University Press, 1959. Pp. 339-427.

23. Rainbird, W. J. "Turbulent Boundary-Layer Growth and Separation on a Yawed Cone," AIAA Journal, 6:2410-2416, December, 1968.

24. Davis, R. T. "Numerical Solution of the Hypersonic Viscous Shock-Layer Equations," AIAA Journal, 8:843-851, May, 1970.

UNCLASSIFIED

Security Classification

DOCUMENT CONTROL DATA - R & D

(Security classification of title, body of abstract and indexing annotation must be entered when the overall report is classified)

1 ORIGINATING ACTIVITY (Corporate author)

Arnold Engineering Development Center
Arnold Air Force Station, Tennessee

2a. REPORT SECURITY CLASSIFICATION

UNCLASSIFIED

2b. GROUP

N/A

3 REPORT TITLE

ANALYSIS OF LAMINAR BOUNDARY LAYERS ON RIGHT CIRCULAR CONES AT ANGLE OF ATTACK, INCLUDING STREAMLINE-SWALLOWING EFFECTS

4 DESCRIPTIVE NOTES (Type of report and inclusive dates)

Final Report - September 1970 to April 1972

5 AUTHOR(S) (First name, middle initial, last name)

Arloe Wesley Mayne, Jr., ARO, Inc.

6 REPORT DATE	7a. TOTAL NO OF PAGES	7b. NO. OF REFS
October 1972	105	24

8a. CONTRACT OR GRANT NO	9a. ORIGINATOR'S REPORT NUMBER(S)
b. PROJECT NO	AEDC-TR-72-134
c. Program Element 65802F	9b. OTHER REPORT NO(S) (Any other numbers that may be assigned this report)
d.	ARO-VKF-TR-72-117

10 DISTRIBUTION STATEMENT

Approved for public release; distribution unlimited.

11 SUPPLEMENTARY NOTES	12 SPONSORING MILITARY ACTIVITY
Available in DDC	Headquarters AEDC, AFSC Arnold AF Station, Tennessee 37389

13 ABSTRACT A method has been developed for treating the three-dimensional compressible laminar boundary-layer equations for the case of a right circular cone at angle of attack in supersonic and hypersonic flow. Swallowing by the boundary layer of the inviscid entropy layer, i.e., streamline swallowing, has been treated by means of a mass-flow balance between the inviscid and viscous flowfields. The boundary-layer equations were developed in a general Crocco-variables form and particularized to the case of a right circular cone at angle of attack. A finite-difference technique was formulated for solving the governing equations and treating the streamline-swallowing phenomenon. The resulting second-order accurate set of coupled nonlinear difference equations were solved in an iteration scheme which employed an efficient algorithm especially suited to their form. The general treatment of the problem and the method of solution were verified by the good agreement obtained between the results of the method developed and both experimental data and results from another method of computation. Results were presented which showed that, for sufficiently high Mach number and bow shock strength variations, streamline swallowing has a significant influence on computed boundary-layer data.

DD FORM 1 NOV 65 1473

UNCLASSIFIED

Security Classification

14. KEY WORDS	LINK A		LINK B		LINK C	
	ROLE	WT	ROLE	WT	ROLE	WT
analyzing						
laminar boundary layers						
cones (right circular)						
streamlining						
supersonic flow						
hypersonic flow						